2480 Ma mafic magmatism in the northern Black Hills, South Dakota: a new link connecting the Wyoming and Superior cratons[1]

Peter S. Dahl, Michael A. Hamilton, Joseph L. Wooden, Kenneth A. Foland, Robert Frei, James A. McCombs, and Daniel K. Holm

Abstract: The Laramide Black Hills uplift of southwest South Dakota exposes a Precambrian crystalline core of ~2560–2600 Ma basement granitoids nonconformably overlain by two Paleoproterozoic intracratonic rift successions. In the northern Black Hills, a 1 km thick, layered sill (the Blue Draw metagabbro) that intrudes the older rift succession provides a key constraint on the timing of mafic magmatism and of older rift-basin sedimentation. Ion microprobe spot analyses of megacrysts of magmatic titanite from a horizon of dioritic pegmatite in the uppermost sill portion yield a $^{207}Pb/^{206}Pb$ upper-intercept age of 2480 ± 6 Ma (all age errors ±2σ), comparable to two-point $^{207}Pb/^{206}Pb$ errorchron ages obtained by Pb stepwise leaching of the same titanites. Nearly concordant domains in coexisting magmatic zircon yield apparent spot ages ranging from 2458 ± 16 to 2284 ± 20 Ma (i.e., differentially reset along U–Pb concordia), and hornblende from an associated metadiorite yields a partially reset date with oldest apparent-age increments ranging between 2076 ± 16 and 2010 ± 8 Ma. We interpret these data as indicating that an episode of gabbroic magmatism occurred at 2480 Ma, in response to earlier rifting of the eastern edge of the Wyoming craton. Layered mafic intrusions of similar thickness and identical age occur along a rifted belt in the southern Superior craton (Sudbury region, Ontario). Moreover, these mafic intrusions are spatially aligned using previous supercontinent restorations of the Wyoming and Superior cratons (Kenorland–Superia configurations). This new "piercing point" augments one previously inferred by spatial–temporal correlation of the Paleoproterozoic Huronian (southern Ontario) and Snowy Pass (southeastern Wyoming) supergroups. We propose that layered mafic intrusions extending from Nemo, South Dakota, to Sudbury, Ontario, delineate an axial rift zone along which Wyoming began to separate from Superior during initial fragmentation of the Neoarchean supercontinent at ≥2480 Ma.

Résumé : Le soulèvement des Black Hills dans le sud-ouest du Dakota du Sud, au cours du Laramide, a exposé un noyau cristallin, ~2560 – 2600 Ma, de granitoïdes du socle sur lesquels reposent, de manière discordante, deux successions paléoprotérozoïques d'effondrement intracratonique. Dans les Black Hills du nord, un filon-couche stratifié d'une épaisseur d'un kilomètre (le métagabbro de Blue Draw), qui recoupe la plus ancienne succession de fossés tectoniques, limite le moment du magmatisme mafique et d'une sédimentation plus ancienne dans le bassin du fossé. Des analyses ponctuelles, par microsonde ionique, de mégacristaux de titanite magmatique d'un horizon de pegmatite dioritique dans la portion supérieure du filon-couche ont donné un âge maximal de recoupement de 2480 ± 6 Ma, déterminé par le rapport $^{207}Pb/^{206}Pb$ (toutes les erreurs d'âge ± 2σ), ce qui est comparable aux âges isochrones $^{207}Pb/^{206}Pb$ à deux points obtenus par lixiviation progressive du Pb de ces titanites. Des domaines presque concordants dans des zircons magmatiques coexistants ont donné des âges ponctuels apparents variant de 2458 ± 16 à 2284 ± 20 Ma (c.-à-d., avec remaniement différentiel le long de la courbe Concordia U–Pb) et une hornblende d'une métadiorite associée a donné un âge de

Received 26 August 2005. Accepted 23 May 2006. Published on the NRC Research Press Web site at http://cjes.nrc.ca on 4 January 2007.

Paper handled by Associate Editor L. Corriveau.

P.S. Dahl.[2] Department of Geology, Kent State University, Kent, OH 44242, USA.
M.A. Hamilton.[3] J.C. Roddick Ion Microprobe (SHRIMP II) Laboratory, Geological Survey of Canada, 601 Booth St., Ottawa, ON K1A 0E8, Canada.
J.L. Wooden. United States Geological Survey, 345 Middlefield Road, Menlo Park, CA 94025, USA.
K.A. Foland. Department of Geological Sciences, The Ohio State University, Columbus, OH 43210, USA.
R. Frei. Geological Institute, University of Copenhagen, Øster Voldgade 10, DK-1350 Copenhagen, Denmark, and NordCEE, Nordic Center for Earth Evolution, Denmark.
J.A. McCombs and D.K. Holm. Department of Geology, Kent State University, Kent, OH 44242, USA.

[1]This paper is one of a selection of papers published in this Special Issue on *The Wyoming Province: a distinctive Archean craton in Laurentian North America*.
[2]Corresponding author (e-mail: pdahl@kent.edu).
[3]Present address: Jack Satterly Geochronology Laboratory, Department of Geology, University of Toronto, Toronto, ON M5S 3B1, Canada.

 doi:10.1139/E06-066

remaniement partiel dont les incréments les plus anciens d'âge apparent varient entre 2076 ± 16 et 2010 ± 8 Ma. Nous interprétons ces données en tant qu'indicateurs d'un épisode de magmatisme gabbroïque associé à la fragmentation de la bordure à l'est du craton de Wyoming, il y a environ 2480 Ma. Des intrusions mafiques stratifiées d'une épaisseur semblable et d'un âge identique se retrouvent le long d'une ceinture d'effondrement dans le craton du lac Supérieur méridional (région de Sudbury, Ontario). De plus, ces intrusions mafiques sont alignées le long d'anciennes restaurations supercontinentales des cratons de Wyoming et du Supérieur (configurations Kenorland–Superia). Ce nouveau « point de percée » en soutient un autre inféré par la corrélation spatio–temporelle des supergroupes de l'Huronien (sud de l'Ontario) et de Snowy Pass (sud-est du Wyoming) au Paléoprotérozoïque. Nous proposons que les intrusions mafiques stratifiées s'étendant de Nemo, au Dakota du Sud, à Sudbury, en Ontario, délimitent une zone d'effondrement axial le long de laquelle le craton de Wyoming a commencé à se séparer du craton du Supérieur au cours de la fragmentation initiale du supercontinent néoarchéen, il y a ≥ 2480 Ma.

[Traduit par la Rédaction]

Introduction

Swarms of mafic dykes and sills, a typical fingerprint of continental rifting, can be used to constrain the timing of supercontinent breakup or attempted breakup (Ernst and Buchan 2001). For instance, intrusion of the 2475–2446 Ma Matachewan–Hearst mafic dyke swarm (Heaman 1997) and the 2490–2475 Ma East Bull Lake (EBL) suite of layered mafic intrusive rocks (James et al. 2002) are widely interpreted as indicating early Paleoproterozoic, mantle-plume driven, intracontinental rifting centered near Sudbury, Ontario, (southern Superior craton) during the onset of Kenorland breakup. Roscoe and Card (1993) envisioned the Wyoming craton as the continental landmass that rifted away from the southern Superior portion of Kenorland, before moving rapidly west and docking with supercontinent Laurentia at ~1850–1715 Ma (Dahl et al. 1999). In this tectonic scenario, the Wyoming craton may be somewhat analogous to Amazonia, a microcontinent that collided with eastern North America during the Mesoproterozoic assembly of supercontinent Rodinia, broke away during the ~800 Ma dispersal of Rodinia, and was ultimately reassembled as part of South America (Weil et al. 1998).

Roscoe and Card (1993) based their pre-2500 Ma Wyoming–Superior reconstruction (Kenorland) largely using a stratigraphic "piercing point", namely the present boundaries of the Paleoproterozoic Snowy Pass and Huronian supergroups exposed in southeastern Wyoming and southern Ontario, respectively. These extensive packages of rift-basin sedimentary rocks are strikingly similar, both having an older (~2450–2100 Ma) epicratonic rift facies succeeded by a ~2100–1800 Ma passive margin sedimentary package. Following this reconstruction, the southeastern Wyoming craton would have lain immediately south of present-day Lake Superior and the north shore of Lake Huron in northern Michigan and southernmost Ontario. More recently, Bleeker (2003) and Bleeker and Ernst (2006) have proposed a somewhat different configuration for Kenorland, referred to as supercraton Superia, in which the eastern Hearne craton was also attached to the southern Superior craton. In the Superia configuration, the Wyoming craton still lies south of the Superior Province, sandwiched between the Hearne craton to the east (Bleeker and Ernst 2006) and the rocks of the Minnesota River Valley (MRV) terrane to the west (Roscoe and Card 1993).

Recent paleomagnetic and geochronological data from the central Wyoming craton support the hypothesis that the Huronian and Snowy Pass supergroups were adjacent to each other at ~2170 Ma and thus may have evolved as a single sedimentary rift basin between ~2450 and 2100 Ma (Harlan et al. 2003*a*). After ~2100 Ma, the Wyoming craton is thought to have rifted away from the southern Superior craton (Roscoe and Card 1993), a scenario that is consistent with occurrence of a 2076–2067 Ma plume centered just south and east of the Superior craton and MRV terrane, respectively (Schmitz et al. 2006).

Other workers, arguing that the Huronian – Snowy Pass time–stratigraphic correlation is not particularly unique in the Proterozoic sedimentary record, consider the Kenorland and Superia configurations as also non-unique. For example, Cox et al. (2000) have proposed that the southeastern Wyoming craton was once connected to the western Slave craton of Canada as part of the pre-2500 Ma supercraton Sclavia (Bleeker and Ernst 2006). These workers proposed this configuration on the basis of occurrences of nearly coeval, 2010–2030 Ma mafic dykes at the margins of both cratons. Moreover, an apparent lack of 2500–2450 Ma mafic igneous rocks in the eastern and southeastern Wyoming craton, but their common occurrence throughout the southern Superior craton, has presented a considerable weakness for any model connecting southeastern Wyoming to southern Superior prior to 2500 Ma.

Laramide uplifts in the eastern and southeastern Wyoming craton provide the only regional exposures of Precambrian crystalline rocks, and therefore represent strategic locations for testing proposed pre-2500 Ma connections between the Wyoming craton and the Superior or Slave cratons. Premo and Van Schmus (1989) confirmed felsic magmatism at ~2430–2450 Ma in the southeastern Wyoming uplifts, but no occurrences of similar age mafic rocks are yet known from this part of the craton. In contrast, the Black Hills Laramide uplift of western South Dakota (Fig. 1), commonly regarded as representing the easternmost exposure of the Archean Wyoming craton (Walker et al. 1986; Gosselin et al. 1988), contains abundant mafic igneous rocks, many of which are of uncertain Paleoproterozoic age (Redden et al. 1990). The largest of these mafic bodies is the focus of this study.

In this study, we present new U–Th–Pb isotopic data for magmatic titanite and zircon from the most prominent mafic intrusive body in the Black Hills crystalline core. Located near Nemo, South Dakota, the Blue Draw metagabbro (BDM)

Fig. 1. Generalized geologic map of the Laramide Black Hills uplift, South Dakota, the crystalline core of which is underlain by Neoarchean basement and Paleoproterozoic cover rocks. Map is modified after DeWitt et al. (1989), Redden et al. (1990), and Dahl et al. (2005*b*). LEG, Little Elk granite gneiss; BFG, Biotite–feldspar gneiss; BMG, Bear Mountain granite (Gosselin et al. 1988). Paleoproterozoic Blue Draw metagabbro (BDM) is located ~2–3 km west of Nemo. Inset (modified after Mueller et al. 2002) shows location of the Black Hills in relation to the Archean Wyoming craton, as well as locations of Wyoming and adjacent Archean cratons within southwestern Laurentia. Paleoproterozoic mobile belts shown are the Trans-Hudson orogen (THO, including the Dakota segment, USA), Great Falls tectonic zone (GFtz), and Vulcan Low (VL). Terminal collisions involving the Wyoming craton during assembly of Laurentia occurred at ~1770–1760 Ma along the GFtz (Mueller et al. 2004; Jones et al. 2004) and at ~1775–1715 Ma along the Dakota segment of the THO (Redden et al. 1990; Dahl et al. 2005*b*). undiff., undifferentiated; incl., includes.

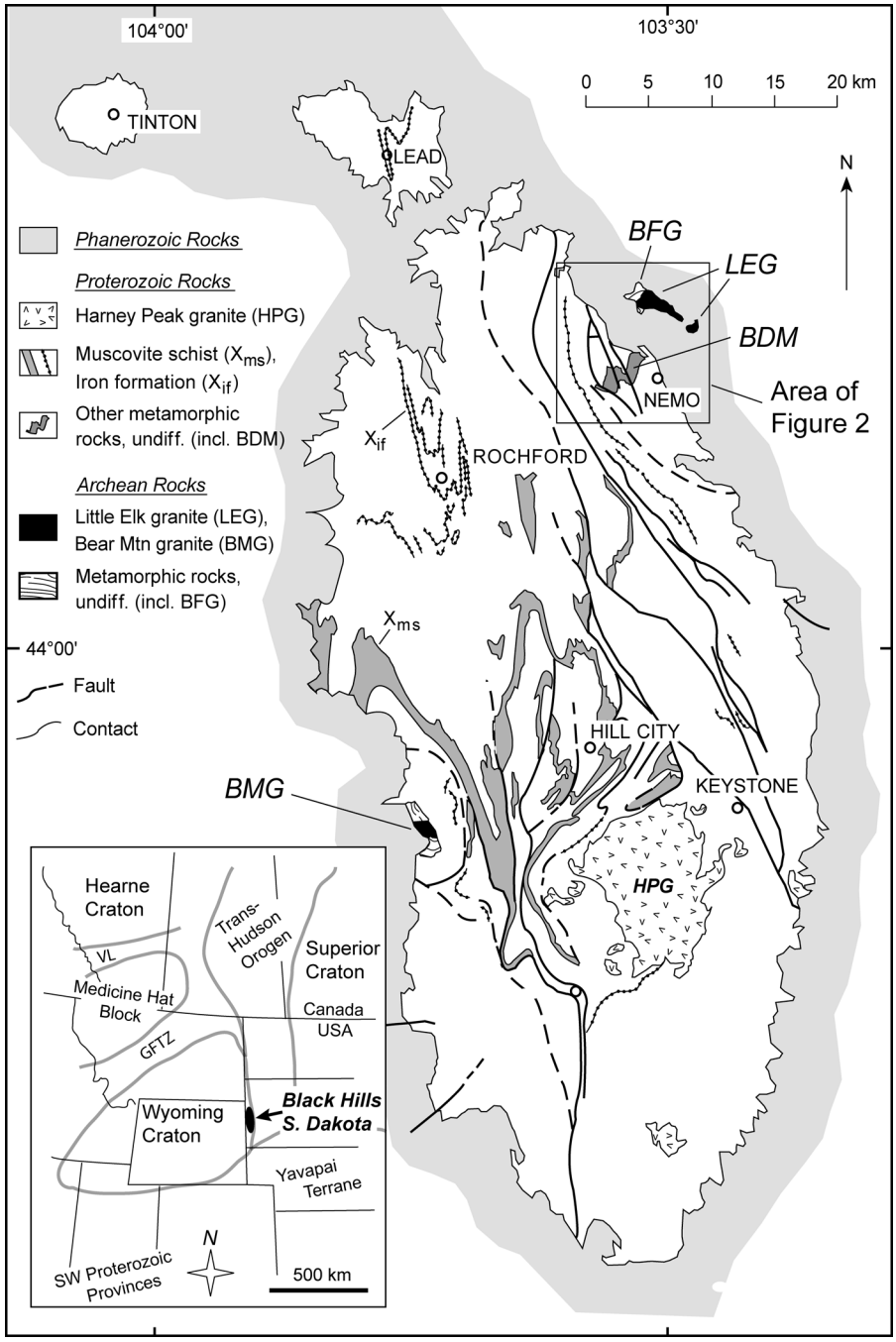

(Fig. 2), is a 1 km thick, layered sill. Its layered structure exposes, from bottom to top, serpentinite, hornblendite, hornblende–plagioclase gabbro to diorite, biotite granodiorite, and discontinuous dioritic pegmatite (Woo 1952; Redden 1981). Based upon an array of highly discordant zircon data from the pegmatite, Redden et al. (1990) reported a U–Pb concordia upper-intercept age of 2170 ± 110 Ma (2σ) for the BDM. We present a concordant magmatic titanite age of

Fig. 2. Detailed geologic map of the Nemo area, northern Black Hills (enlargement of boxed area in Fig. 1), modified after DeWitt et al. (1989), Redden et al. (1990), Bekker et al. (2003), and Dahl and McCombs (2005). Map shows distributions of the Blue Draw metagabbro (BDM), associated lithologies, and the Estes unconformity (EU). metaconglom., metaconglomerate; Pz, Paleozoic; Qal, Quaternary alluvium. Within the uppermost BDM are shown the locations of samples chosen for study. Dioritic pegmatite sample JAM-14a and equivalent sample Z-3a of Redden et al. (1990) were selected for $^{207}Pb/^{206}Pb$ dating of titanite and zircon, whereas metadiorite sample BD-5 was selected for $^{40}Ar/^{39}Ar$ dating of hornblende. T.N., true north; M.N., magnetic north. See text for results and discussion.

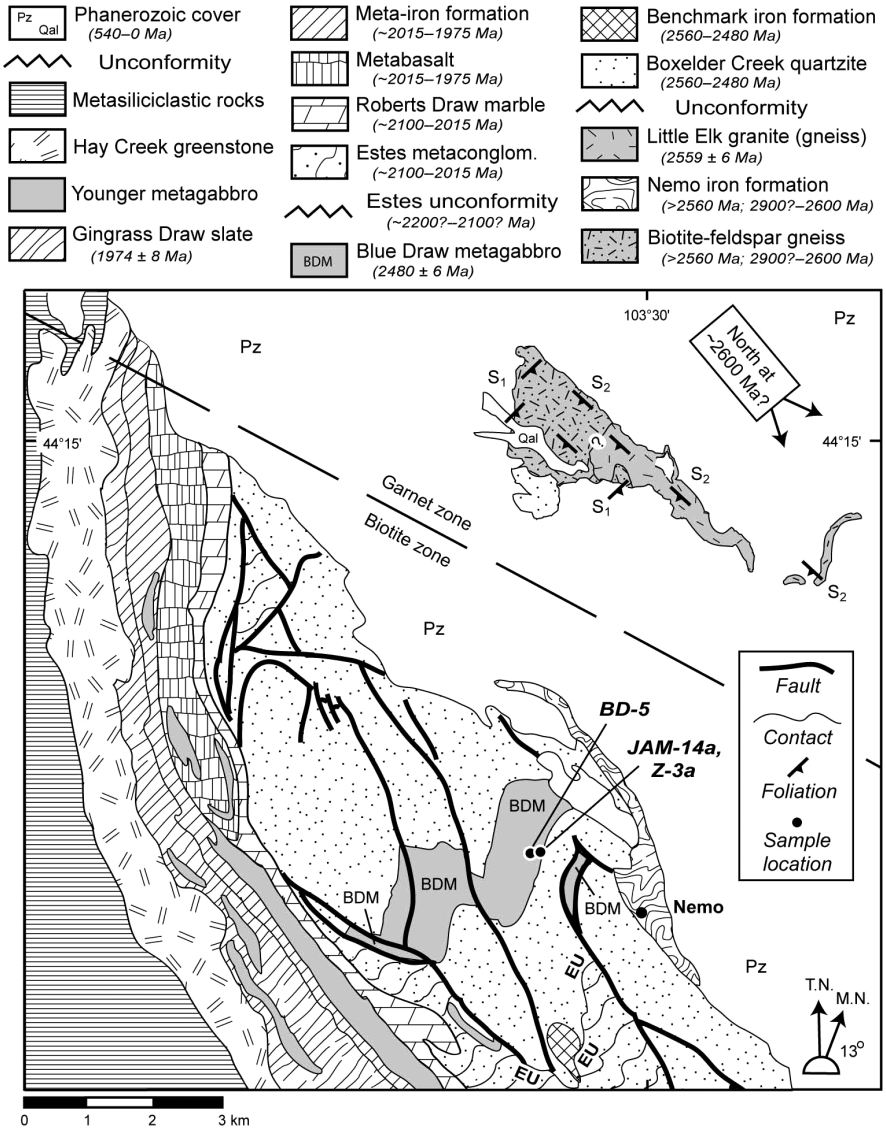

2480 ± 6 Ma (±2σ) from the same unit, indicating that Paleoproterozoic rift-related sedimentation in the easternmost Wyoming craton is significantly older than previously recognized. This 2480 Ma age ostensibly precludes a Wyoming–Slave connection because rift-related mafic rocks of this age are not recognized in the Slave craton (Bleeker and Ernst 2006). Instead, our result potentially provides an important new link connecting the eastern Wyoming craton to the southern Superior Province.

Geologic and geochronologic setting

The Archean Wyoming Province (inset, Fig. 1) is bounded on its north, east, and southeast margins by Paleoproterozoic orogenic belts that were active when the craton collided with southwestern Laurentia between ~1865 and 1715 Ma (Frost 1993; Chamberlain 1998; Dahl et al. 1999, 2000, 2005*a*, 2005*b*; Mueller et al. 2002, 2004; Roberts et al. 2002). The Black Hills constitute a Laramide domal uplift located at the eastern margin of the Wyoming craton (Fig. 1). The core of the dome exposes Precambrian metaigneous and metasedimentary rocks ranging from biotite- to second-sillimanite grade. Neoarchean basement exposed in the northeast and west-central Black Hills (Figs. 1, 2) consists mostly of syntectonic granitoids intruded into older gneiss. The isotopic and trace-element signatures of these granitoids suggest that the Black Hills are part of the Wyoming craton (Gosselin et al. 1988; Walker et al. 1986), as shown in Fig. 1 (inset), and not the Superior craton. Neoarchean units (Figs. 1, 2; Gosselin et al. 1988) include the Nemo Iron Formation; a biotite–feldspar

gneiss (BFG); the 2559 ± 6 Ma Little Elk granite (LEG), which intrudes the BFG; and the 2595 ± 11 Ma granite at Bear Mountain to the south (McCombs et al. 2004). The age of the BFG is uncertain, and it appears to have both magmatic and sedimentary protoliths (Gosselin et al. 1988). However, xenocrysts of 2894 ± 6 Ma magmatic zircon found in a 2563 ± 6 Ma orthogneiss constrain a maximum protolith age for this component of the BFG (McCombs et al. 2004). Thus, Dahl and McCombs (2005) suggested that the paragneiss component of the BFG was originally deposited on a ~2900 Ma basement that is no longer exposed (likewise for the associated Nemo Iron Formation, Fig. 2).

Two Neoarchean deformational fabrics are recognized in the BFG–LEG complex. The BFG exhibits both a northeast-trending (S_1) and a northwest-trending (S_2) fabric (Fig. 2), whereas the LEG exhibits only the younger S_2 fabric (Gosselin et al. 1988). The S_1 fabric parallels sedimentary layering in the BFG and was likely developed between ~2900(?) and 2560 Ma (Dahl and McCombs 2005), whereas the S_2 fabric imposed during the LEG intrusion is precisely dated at 2560 Ma (Gosselin et al. 1988; McCombs et al. 2004).

The Neoarchean basement complex is overlain by two main rift successions, both consisting of Paleoproterozoic sedimentary and igneous rocks. On the basis of bulk U–Pb ages of zircon in interlayered mafic igneous rocks and intermediate tuffs, Redden et al. (1990) loosely bracketed their depositional ages between ~2550 Ma (Gosselin et al. 1988) and 1880 Ma. The two rift successions are separated in both space and time by the Estes unconformity (EU) (Nemo area, Fig. 2), an erosional surface that postdates BDM intrusion and predates structural overturning as described by Redden (1981, 1987). The younger, areally predominant rift succession (Figs. 1, 2) is a thick package of metamorphosed conglomerates, carbonates, iron formations, greywackes, pelites, alkalic tuffs, basalts, and gabbros (Redden et al. 1990). Dahl and McCombs (2005) proposed that deposition of this younger suite is bracketed from ~2100–1880 Ma, on the basis of published geochronology and chemostratigraphy (Bekker et al. 2003). The older rift-related suite, confined to the Nemo area and intruded by the BDM (Figs. 1, 2), comprises a sequence of metamorphosed conglomerate, sandstone, and iron formation (Redden et al. 1990).

The BDM layered sill was (1) intruded into horizontal (Boxelder Creek) sandstone and (Benchmark) Iron Formation (Fig. 2); (2) differentiated horizontally upon cooling and solidification; (3) possibly folded (with the older sedimentary rocks) on a northwest-trending axis; (4) nonconformably overlain by the younger rift succession, atop the EU; (5) structurally overturned (with the unconformity and adjacent sedimentary rocks) on an approximate northeast–southwest-trending axis; and (6) (re-) folded on a northwest-trending axis (with the unconformity and adjacent sedimentary rocks) during the Wyoming–Superior collisional orogeny, D_2 (Redden 1987; DeWitt et al. 1986, 1989; Redden et al. 1990; Dahl et al. 1999; Dahl and McCombs 2005). These events are summarized in the geologic map (Fig. 2), from which it is possible to gain a stratigraphic and structural cross-section of the Nemo area by viewing the map upside down (Redden 1987).

Neoarchean basement and Paleoproterozoic cover rocks in the Black Hills were subjected to at least three to five thermotectonic events between ~1850 and 1650 Ma, associated with initial convergence and terminal collision of the Wyoming craton and adjacent terranes to form southwest Laurentia. The main Paleoproterozoic structural elements preserved in these rocks include east-northeast-trending fold nappes (F_1) and thrusts that were refolded into the north-northwest-trending upright folds (F_2) shown in Fig. 1. Associated with these large-scale folds is a steep, locally penetrative, north-northwest-trending, axial planar foliation (Paleoproterozoic S_2). Respectively, these structures resulted from a northwest-directed accretion of the northern Yavapai island-arc terrane at ~1775 Ma, from the south (D_1), and from an approximately east–west shortening associated with Wyoming–Superior continental collision (D_2) at ~1750–1715 Ma (Dahl et al. 1999, 2005*a*, 2005*b*). Localized doming (D_3) at 1715 Ma accompanied late syn- to post-collisional intrusion of the Harney Peak leucogranite and associated pegmatites into the mid-crust, which then cooled slowly for ~400 million years (Holm et al. 1997). The Precambrian crystalline core was exhumed to the surface prior to ~520 Ma (nonconformable onlap of Cambrian strata) and was re-exposed during a period of Laramide uplift and associated magmatism dated at ~60 Ma (Lisenbee 1978).

Samples and analytical methods

The Boxelder Creek sandstone and overlying, younger Benchmark Iron Formation were both intruded by the younger BDM sill, followed by development of the EU and the subsequent deposition of Estes conglomerate (legend, Fig. 2). Therefore, establishing an accurate and precise intrusive age of the BDM is fundamental to bracketing both the depositional timeframe of the older rift succession and the younger erosional timeframe represented by the EU.

Accordingly, both dioritic pegmatite and underlying metadiorite in the uppermost Blue Draw layered sill were sampled for titanite and zircon, and for hornblende, respectively. These upper horizons were targeted for isotopic analysis of magmatic minerals on the expectation that gravity differentiation following BDM intrusion would have pre-concentrated radioactive large-ion lithophile elements therein (e.g., K, Rb, U, Th, etc.). The initial objective was to obtain an accurate and precise age within one mineral-isotopic system that could be verified by at least one other age obtained in another system. The dioritic pegmatite (samples JAM-14a and Z-3a, Fig. 2) contains the assemblage plagioclase, quartz, titanite, hornblende, biotite, and accessory rutile and zircon. The metadiorite (sample BD-5, Fig. 2) contains mostly ferro-hornblende rimmed by ferro-tschermakitic hornblende, plus plagioclase and quartz (Redden 1981, 1987). The two rock samples were crushed and sieved to grain sizes ranging from >400 to 400–40 μm to extract several megacrysts of titanite and to obtain high-quality zircon and hornblende separates using heavy liquid and magnetic separation methods, respectively. The titanite and zircon grains were analyzed isotopically by sensitive high-resolution ion microprobe (SHRIMP) at the Stanford US Geological Survey facility, Menlo Park, and the Geological Survey of Canada, Ottawa, respectively. A bulk titanite population was further analyzed isotopically by Pb stepwise leaching (PbSL) at the University of Copenhagen, Copenhagen, and a bulk hornblende population was analyzed

Table 1. Isotopic data (Pb stepwise leaching (PbSL)) for titanite megacrysts in dioritic pegmatite (sample Z-3a).

Acid	Time	Code[a]	$\frac{^{206}Pb}{^{204}Pb}$	±1σ	$\frac{^{207}Pb}{^{204}Pb}$	±1σ	$\frac{^{208}Pb}{^{204}Pb}$	±1σ	r_1	r_2
mix	20 min	[1]	48.58	0.04	19.26	0.02	83.67	0.08	0.99	0.96
1N HBr	1 h	[2]	82.25	0.04	23.40	0.01	128.79	0.07	0.96	0.94
4N HBr	3 h	[3]	291.90	0.86	56.33	0.17	238.23	0.71	1.00	1.00
8.8N HBr	12 h	[4]	457.56	2.85	85.50	0.54	429.52	2.68	1.00	1.00
8.8N HBr	48 h	[5]	399.70	1.80	76.56	0.35	424.20	1.92	1.00	1.00
residue	–	[6]	471.73	2.66	82.55	0.47	403.78	2.28	1.00	1.00

Note: r_1, $^{206}Pb/^{204}Pb$ vs. $^{207}Pb/^{204}Pb$ error correlation (Ludwig 2003); r_2, $206Pb/^{204}Pb$ vs. $^{208}Pb/^{204}Pb$ error correlation (Ludwig 2003); min, minutes; h, hours.

[a]Corresponds to data point labels in Fig. 3.

by Ar incremental-release methods at the Radiogenic Isotope Laboratory located at The Ohio State University, Columbus.

Pb stepwise-leaching methodology (titanite)

PbSL procedures followed the recipes developed by Frei and Kamber (1995). The mechanisms of successive leaching, by increasingly stronger acids, of common (i.e., unsupported) and radiogenic Pb components in individual mineral phases have been documented by Frei et al. (1997). Parallel studies of applied PbSL schemes (Schaller et al. 1997; Dahl and Frei 1998; Dahl et al. 2005*a*) have demonstrated the ability of this technique to reveal the presence and mean ages of U–Th-bearing accessory phases, which often are contained as minute inclusions in the host minerals. The types of acids used in the PbSL experiment of titanite in this study and the exposure times of the successively leached titanite separate are contained in Table 1 and coded respectively. Pb was separated from the leach solutions by applying a conventional HBr–HCl elution procedure on DOWEX AG-1 × 8 anion resin, first using 0.5 mL glass stem columns and then, mainly to purify the Pb fractions, 300 μL glass stem columns loaded with the respective resin. The isotopic composition of Pb was measured on a VG Sector 54 IT mass spectrometer at the Geological Institute, University of Copenhagen, using a static multi-collection routine. Procedural blanks remained below ~80 pg of Pb, which, judging by comparison with Pb beam intensities of the respective sample fractions, can be neglected in terms of having significant influence on the measured Pb isotopic compositions of the samples. Data were corrected for instrumental Pb fractionation of 0.103 ± 0.002% per atomic mass unit, assessed through repeated monitoring of the NBS 981 Pb standard. The respective error is included into the error propagation of the individual Pb isotopic ratios of the samples. Long-term reproducibility of ~500 ppm (2σ) is obtained for the NBS 981 Pb standard.

SHRIMP methodology (titanite)

U–Th–Pb analyses of two ~1.3 mm × 0.8 mm grains of titanite were conducted on the SHRIMP-RG ion microprobe in the SUMAC facility at Stanford University. The titanites, along with fragments of a standard, were mounted on double-stick tape on glass slides in 1 mm × 6 mm rows, cast in epoxy, and ground and polished to a 1 μm finish on a 25 mm diameter × 4 mm thick disc. All grains were imaged with transmitted light and reflected light on a petrographic microscope, and with backscattered mode on a JEOL 5600 scanning electron microscope, to identify internal structure, inclusions, and physical defects. The mounted grains were washed with 1N HCl and distilled water, dried in a vacuum oven, and coated with Au. Secondary ions were generated from the target spot with an O^- primary ion beam varying from 4 to 6 nA. The primary ion beam typically produces a spot with a diameter of 20–40 μm and a depth of 1–2 μm for an analysis time of 9–12 min. Nine peaks were measured sequentially: $^{40}Ca^{48}(Ti,Ca)_2{}^{16}O_4$, ^{204}Pb, background (0.050 mass units above ^{204}Pb), ^{206}Pb, ^{207}Pb, ^{208}Pb, ^{238}U, $^{248}Th^{16}O$, and $^{254}U^{16}O$. Concentration and age data for titanites as reported in Table 2 were standardized against reference titanite BLR-1 (age = 1051 Ma, mean U concentration = 250 ppm; John Aleinikoff, personal communication), which was analyzed repeatedly throughout the duration of the analytical session. Data reduction followed methods described by Williams (1997) and Ireland and Williams (2003) and used the SQUID and Isoplot programs (Ludwig 2001, 2003). Correction of the measured isotopic ratios for common Pb was estimated from monitored ^{204}Pb counts.

SHRIMP methodology (zircon)

Zircon grains from pegmatite sample JAM-14a were arranged along with fragments of the Geological Survey of Canada laboratory zircon reference standard (BR266/z6266: 910 ppm U, $^{206}Pb/^{238}U$ isotope dilution age = 559 Ma), cast in an epoxy grain mount, and polished sufficiently with diamond compound to reveal the grain centers. The mount was then cleaned, coated with approximately 10 nm of high-purity Au, and individual zircon grains were imaged with a Cambridge Instruments S360 scanning electron microscope equipped with cathodoluminescence and back-scattered electron (BSE) detectors to identify internal compositional zoning, cracks, and inclusions. U–Pb isotopic spot analyses of the zircon were carried out with the Geological Survey of Canada SHRIMP II, following the general methods described by Stern (1997) and Hamilton et al. (2004). Highest-quality zircon grains in this sample comprised short but cloudy magmatic prisms with remnants of oscillatory zoning and elongate forms resembling the skeletal morphologies sometimes found in mafic pegmatites. Most grains contain inclusions of quartz or feldspar and are very commonly cracked. An ubiquitous feature of almost all grains is a pervasive, micron-scale, "pitted" texture suggestive of post-crystallization partial dissolution and (or) alteration accompanying a period of enhanced fluid flow. Obtaining the best quality results from the remaining

Table 2. Isotopic data (SHRIMP) for titanite and zircon grains in dioritic pegmatite (sample JAM-14).

Phase and Grain spot	U (ppm)	Th (ppm)	Th/U	Pb* (ppm)	$^{206}Pb/^{204}Pb$	f_{206}%	$^{206}Pb/^{238}U$	±1σ	$^{207}Pb/^{235}U$	±1σ	R	$^{207}Pb/^{206}Pb$	±1σ	Apparent ages (±1σ, Ma) $^{206}Pb/^{238}U$	$^{207}Pb/^{235}U$	$^{207}Pb/^{206}Pb$	Disc. (%)
Titanite																	
1.1	106	239	2.2	42.7	8330	0.20	0.4657	0.0143	10.4727	0.3263	0.983	0.1631	0.0009	2465±63	2478±28	2488±10	1.0
1.2	37	76	2.0	13.9	11360	0.15	0.4333	0.0135	9.7347	0.3165	0.96	0.1629	0.0015	2321±61	2410±28	2486±15	7.1
1.3	101	232	2.3	37.5	37040	0.05	0.4328	0.0102	9.6529	0.2345	0.971	0.1617	0.0009	2319±46	2402±22	2474±10	6.7
1.5	67	195	2.9	26.4	37040	0.05	0.4574	0.0126	10.1504	0.2872	0.976	0.1610	0.0010	2428±56	2449±26	2466±10	1.6
1.6	72	201	2.8	26.9	52630	0.03	0.4343	0.0151	9.7003	0.3421	0.986	0.1620	0.0009	2325±68	2407±32	2477±10	6.5
1.7	94	194	2.1	36.0	16130	0.10	0.4451	0.0107	9.9988	0.2493	0.967	0.1629	0.0010	2373±48	2435±22	2486±11	4.8
1.8	112	246	2.2	44.6	n.d.	n.d.	0.4646	0.0122	10.4425	0.2780	0.985	0.1630	0.0008	2460±54	2475±24	2487±8	1.1
1.9	130	288	2.2	51.0	1640	1.04	0.4526	0.0103	10.0813	0.2942	0.777	0.1616	0.0030	2407±46	2442±21	2472±31	2.7
2.1	31	160	5.1	11.2	3570	0.48	0.4117	0.0133	9.0661	0.3131	0.937	0.1597	0.0019	2223±61	2345±29	2453±20	10.4
2.2	36	162	4.6	14.2	3570	0.48	0.4626	0.0144	10.2468	0.3352	0.951	0.1606	0.0016	2451±63	2457±28	2462±17	0.5
2.3	57	289	5.1	20.4	7690	0.22	0.4182	0.0112	9.3186	0.2594	0.962	0.1616	0.0012	2253±51	2370±24	2472±13	9.8
2.4	79	381	4.8	30.0	10870	0.16	0.4428	0.0115	9.9622	0.2690	0.965	0.1632	0.0012	2363±52	2431±24	2489±12	5.3
2.5	23	139	6.0	8.5	4350	0.44	0.4318	0.0117	9.6079	0.3978	0.956	0.1614	0.0020	2314±77	2398±36	2470±21	6.7
2.6	25	146	5.8	9.9	n.d.	n.d.	0.4568	0.0164	10.2265	0.3832	0.960	0.1624	0.0017	2426±73	2455±33	2480±18	2.3
2.7	37	215	5.8	13.6	3450	0.49	0.4245	0.0133	9.3264	0.3121	0.939	0.1593	0.0018	2281±60	2371±28	2449±20	7.3
2.8	32	167	5.3	10.9	21740	0.08	0.4003	0.0139	9.0285	0.3235	0.969	0.1636	0.0015	2170±64	2341±32	2493±15	14.9
Zircon																	
1.1	505	94	0.19	222	59102	0.03	0.4221	0.0058	8.9817	0.1417	0.914	0.1543	0.0010	2270±26	2336±15	2394±11	6.1
1.2	484	207	0.44	250	100000	0.02	0.4693	0.0061	10.1776	0.1531	0.917	0.1573	0.0010	2480±27	2451±14	2427±10	–2.7
1.3	510	99	0.20	227	25297	0.07	0.4264	0.0049	8.8259	0.1186	0.909	0.1501	0.0009	2290±22	2320±12	2347±10	2.9
1.4	557	162	0.30	253	33201	0.05	0.4241	0.0062	9.1677	0.1520	0.933	0.1568	0.0009	2279±28	2355±15	2421±10	7.0
2.1	610	216	0.37	328	32584	0.05	0.4958	0.0072	10.9530	0.1735	0.953	0.1602	0.0008	2596±31	2519±15	2458±8	–6.8
2.2	686	243	0.37	318	103627	0.02	0.4298	0.0056	8.7993	0.1313	0.925	0.1485	0.0009	2305±25	2317±14	2329±10	1.2
3.1	673	466	0.72	368	26497	0.07	0.4689	0.0075	9.9520	0.1714	0.960	0.1540	0.0008	2479±33	2430±16	2390±8	–4.5
4.1	716	337	0.49	331	41964	0.04	0.4184	0.0058	8.3488	0.1298	0.935	0.1447	0.0008	2253±26	2270±14	2284±10	1.6
5.1	689	418	0.63	342	35112	0.05	0.4355	0.0074	8.8739	0.1607	0.965	0.1478	0.0007	2331±33	2325±17	2320±8	–0.5
6.1	711	427	0.62	377	32331	0.05	0.4650	0.0073	9.8477	0.1655	0.963	0.1536	0.0007	2462±32	2421±16	2386±8	–3.8

Note: Measured isotopic ratios and calculated radiometric ages are corrected for common Pb, as estimated from monitored counts of ^{204}Pb. Pb*, radiogenic Pb; f_{206}%, percent ^{206}Pb contribution from common Pb; *R*, error correlation coefficient; Disc., percent discordance along a chord to the origin; n.d., not determined.

Table 3. $^{40}Ar/^{39}Ar$ analytical results for hornblende in diorite (sample BD-5).

T^a	$\frac{^{40}Ar}{^{39}Ar}$ ^{b}	$\frac{^{38}Ar}{^{39}Ar}$ ^{b}	$\frac{^{37}Ar}{^{39}Ar}$ ^{b}	$\frac{^{36}Ar}{^{39}Ar}$ ^{b} (×100)	F^c	$^{39}Ar^d$ (%)	$^{40}Ar^{*e}$ (%)	K/Ca^f	K/Cl^g	Apparent age (Ma)^h
BD-5 hornblende Run #62B67 (J = 0.016100; wt. = 3.48 mg; 0.82 wt.% K)										
600	661.2	0.5276	2.226	10.42	632.3	0.51	95.36	0.234	10.2	4355±38
750	231.3	0.1780	2.652	7.926	208.6	3.76	89.89	0.197	31.9	2656±8
850	92.34	0.0797	0.3247	0.2253	91.72	9.14	99.30	1.61	65.8	1636±4
900	88.51	0.0827	0.5291	0.7421	86.38	5.19	97.54	0.988	64.2	1572±7
940	92.52	0.1275	1.260	0.5192	91.15	5.41	98.38	0.414	41.2	1629±5
970	105.7	0.3012	3.520	1.004	103.3	2.78	97.27	0.148	17.4	1767±9
1000	128.4	0.4349	4.998	1.570	124.6	3.69	96.47	0.104	12.0	1986±9
1010	136.2	0.5596	5.549	1.037	134.2	3.66	97.85	0.094	9.30	2076±8
1020	127.8	0.7587	6.072	0.6117	127.1	9.03	98.73	0.085	6.84	2010±4
1030	128.1	0.9095	6.031	0.3975	128.1	15.01	99.26	0.086	5.70	2019±4
1040	122.1	0.9576	5.850	0.4433	122.0	12.62	99.12	0.089	5.42	1960±4
1060	113.1	0.8321	4.798	0.4519	112.6	8.98	99.00	0.108	6.24	1866±4
1070	103.1	0.5074	3.822	1.215	100.1	2.85	96.64	0.136	10.3	1732±10
1085	94.47	0.3797	3.882	1.458	90.69	2.04	95.54	0.134	13.8	1624±13
1100	94.97	0.4146	5.231	1.764	90.45	1.99	94.62	0.099	12.6	1621±13
1120	99.57	0.5030	7.020	1.848	95.06	1.99	94.64	0.074	10.4	1675±12
1140	99.70	0.5524	7.574	1.960	94.94	1.72	94.33	0.068	9.42	1673±13
1160	116.5	0.7315	7.535	3.707	106.7	1.11	90.75	0.069	7.14	1804±22
1180	105.0	0.6207	6.855	9.016	79.21	0.47	74.78	0.076	8.57	1483±51
1200	114.1	0.7993	6.999	4.626	101.5	1.01	88.19	0.074	6.55	1747±22
1230	110.5	0.6756	6.819	8.458	86.40	0.58	77.53	0.076	7.85	1573±40
1260	116.5	0.8689	6.741	7.654	94.92	0.60	80.77	0.077	6.06	1673±37
1300	124.1	0.8579	7.239	5.792	108.1	0.94	86.37	0.072	6.11	1819±25
1400	124.0	0.7952	7.682	2.225	118.8	4.52	94.85	0.067	6.54	1928±7
Integrated	121.3	0.5969	4.617	1.464	117.8	100	96.55	0.113	8.74	1918

[a]Temperature in °C measured with a thermocouple on the outside of the Ta crucible.

[b]The isotope ratios given are not corrected for Ca-, K-, and Cl-derived Ar isotopic interference, but ^{37}Ar is corrected for decay using a half-life of 35.1 days. The ratios are corrected for line blanks.

[c]F is the ratio of radiogenic ^{40}Ar to K-derived ^{39}Ar. It is corrected for atmospheric Ar and interfering nuclear reactions using the following factors: $(^{40}Ar/^{36}Ar)_{air}$ = 295.5; $(^{38}Ar/^{39}Ar)_K$ = 0.01185; $(^{38}Ar/^{37}Ar)_{Ca} = 3.50 \times 10^{-5}$; $(^{36}Ar/^{38}Ar)_{Cl} = 2.018 \times 10^{-4}$ per day after irradiation; $(^{39}Ar/^{37}Ar)_{Ca} = 6.681 \times 10^{-4}$; $(^{36}Ar/^{37}Ar)_{Ca} = 2.642 \times 10^{-4}$; $(^{40}Ar/^{39}Ar)_K$ = 0.024221.

[d]Relative percent of the total ^{40}Ar released in the fraction.

[e]Percent of the total ^{40}Ar in the fraction that is radiogenic.

[f]Weight ratio calculated using the relationship $K/Ca = 0.523 \times (^{39}Ar_K/^{37}Ar_{Ca})$.

[g]Weight ratio calculated using the relationship $K/Cl = 5.22 \times (^{37}Ar_K/^{38}Ar_{Cl})$.

[h]Ages calculated with a total decay constant of 5.543×10^{-10} year^{-1}. "Integrated" indicates the calculated values for all fractions combined. All uncertainties are given at the 1σ level. An overall systematic uncertainty of ±1% assigned to all ages to allow for uncertainty in the monitor age. The monitor used was a intra-laboratory biotite standard (AL-1) that has a $^{40}Ar/^{39}Ar$ age of 443.5 Ma; an uncertainty of ±1% is assigned to this age to allow for uncertainties in the standards against which AL-1 was calibrated. The age for this monitor was determined by simultaneous cross calibration with several monitors including the Fish Canyon tuff biotite standard (FCT-3) with an age of 27.84 Ma.

unaltered or unfractured domains required the use of a primary beam of sufficient size to effect a sputtering diameter no larger than 15 μm × 20 μm. A primary O^- beam current of roughly 3 nA was used during this session whereas mass resolution was ~5500.

Peak count rates were measured sequentially over nine mass stations for Zr^+, Pb^+, U^+, and Th^+ (plus background and oxides) averaged through six scans, using an electron multiplier in pulse-counting mode (24 ns deadtime). The 1σ uncertainties in the zircon Pb/U ratios shown in Table 2 reflect in part an external error of ±1.0% resulting from the within-session calibration of the BR266 zircon standard (Stern and Amelin 2003). Correction of the measured isotopic ratios for common Pb was estimated from monitored ^{204}Pb counts; in all cases the background-corrected ^{204}Pb counts were low and an independently determined surface blank composition was assumed (Stern 1997).

$^{40}Ar/^{39}Ar$ methodology (hornblende)

Incremental step heating was performed on a hornblende separate extracted from hornblende diorite sample BD-5. The rock was crushed and sieved (to a 250–350 μm size fraction), and the hornblende was separated using standard techniques followed by handpicking. The $^{40}Ar/^{39}Ar$ analyses (Table 3) were performed in the Radiogenic Isotopes Laboratory at The Ohio State University, Columbus, using procedures that have been described previously (Foland 1983; Foland et al. 1984, 1993), except that Ar measurements were made using

Fig. 3. Pb stepwise leaching (PbSL) plots for megacrystic titanite separated from dioritic pegmatite, sample Z-3a. All data are from Table 1 and are plotted with 2σ error ellipses (most of which are smaller than the data point symbols). (*a*) Plot of $^{207}Pb/^{204}Pb$ vs. $^{206}Pb/^{204}Pb$ in six leach steps (uranogenic plot). (*b*) Plot of $^{208}Pb/^{204}Pb$ vs. $^{206}Pb/^{204}Pb$ in the same leach steps (thorogenic plot). Steps 1–6 represent mixing lines of common Pb (lower steps) and relatively radiogenic Pb (upper steps), whereas steps 1–5 and step 6 preferentially leach host titanite (mostly) and included zircon, respectively. SD, South Dakota; MSWD, mean square of the weighted deviation. See text for discussion.

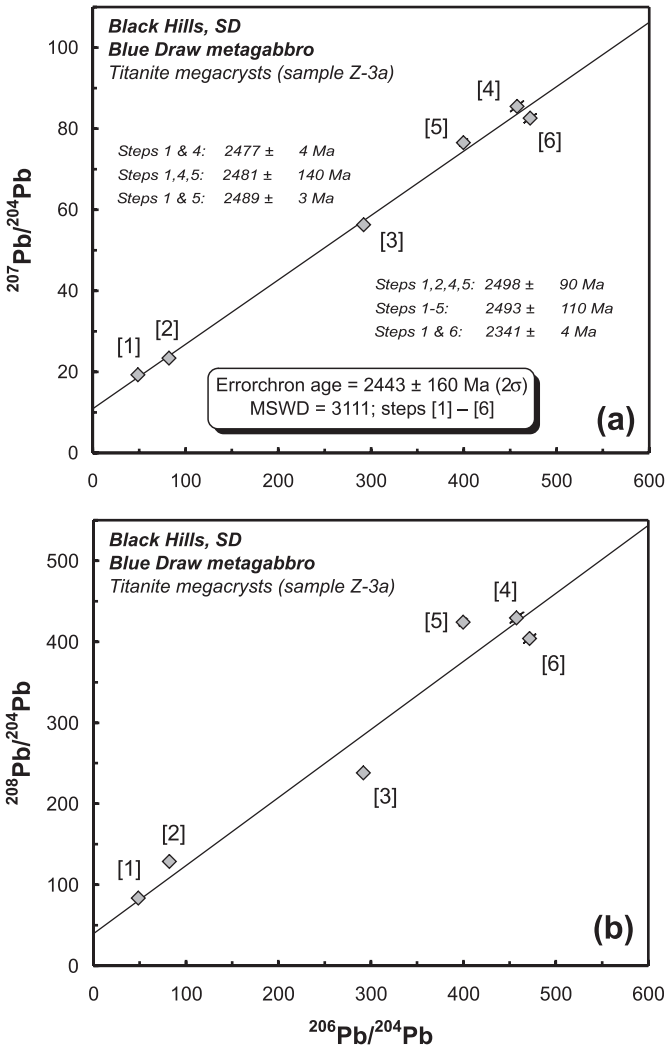

a new mass spectrometer and associated lines. A 3.48 mg aliquot was irradiated in the Ford Nuclear Reactor (University of Michigan, Ann Arbor) and then step-heated in a high-vacuum, low-blank, double-vacuum furnace to successively higher temperatures for a period of approximately 30 min at each step.

Results

This section presents the U–Th–Pb isotopic data obtained for titanite and zircon in the dioritic pegmatite horizon of the uppermost BDM and the K–Ar isotopic data obtained for hornblende in the adjacent metadiorite. Results obtained by PbSL of the bulk titanite separate are summarized in Table 1, and the corresponding PbSL spectra are presented in Fig. 3. The U–Th–Pb data obtained by SHRIMP spot analysis of individual titanite and zircon grains are summarized in Table 2, and U–Pb concordia plots of the data for these respective minerals are presented in Figs. 4*a* and 4*b*. The Ar-isotopic data obtained by incremental release heating of the bulk hornblende separate are given in Table 3 and plotted in Fig. 5.

For all dated minerals, isotopic ratios and ages are listed with 1σ analytical errors in Tables 1–3, whereas ages discussed in the text and shown as intercepts of statistical regressions on concordia diagrams are reported with 2σ errors (95% confidence). Concordia diagrams were created and data regressions carried out using the Isoplot for Excel program of Ludwig (2003).

Titanite

Titanite grains in the upper, dioritic-pegmatite horizon of the BDM are brown, randomly oriented, subhedral to euhedral, and megacrystic (suggesting a magmatic origin). Individual grains display petrographic and BSE evidence for two growth generations in which texturally older interiors are reddish brown and BSE-bright whereas younger clear rims are BSE-darker. Electron microprobe analysis of the grains reveals modest core-to-rim depletion in minor Fe and antithetic enrichment in minor Al with cationic Al/Fe ratios ranging from 1.2 (core) to 0.6 (rim), and abundances of minor Ce_2O_3 and trace Nb_2O_5 ranging from 0.3–0.5 to 0.00–0.05 wt.%, respectively (McCombs 2002). SHRIMP analyses of individual megacrysts revealed a pronounced intergranular variability in Th/U ratio, ranging from 2.1–3.0 (grain 1, Table 2) to 4.7–6.2 (grain 2, Table 2). These Th/U, Al/Fe, Ce, and Nb signatures consistently indicate a magmatic rather than metamorphic origin for the BDM titanite, according to the discriminant criteria established by Aleinikoff et al. (2002) and Wintsch et al. (2005).

As shown in Fig. 4*a*, these titanites are well behaved in terms of their U–Pb isotopic distributions, compared with the relatively disturbed zircons occurring in the same horizon (Fig. 4*b*); this may reflect titanite's relative ability to continually repair radiation damage by an annealing process. The reason for this apparent difference in annealing behavior is that metal-oxygen bonds in zircon are short and strong, thereby inhibiting recrystallization, whereas these bonds in titanite are longer and weaker, which tends to promote this process (Dahl 1997).

For the reasons given earlier in the text, these igneous titanite megacrysts represent excellent candidates for pinpointing the intrusive age of the BDM layered sill. Moreover, their occurrence in the BDM most likely reflects primary growth (cf. Frost et al. 2000), and their Pb closure temperature probably exceeded 700 °C (Cherniak 1993; Dahl 1997) upon fast cooling of the BDM against cold country rock. However, BSE imagery of the megacrysts revealed the presence of minor, minute, and scattered inclusions of zircon. Low metamorphic grade in the Nemo area (Fig. 2) and the morphology of these included zircons suggest that they are not metamorphic, but rather igneous in origin. Special efforts

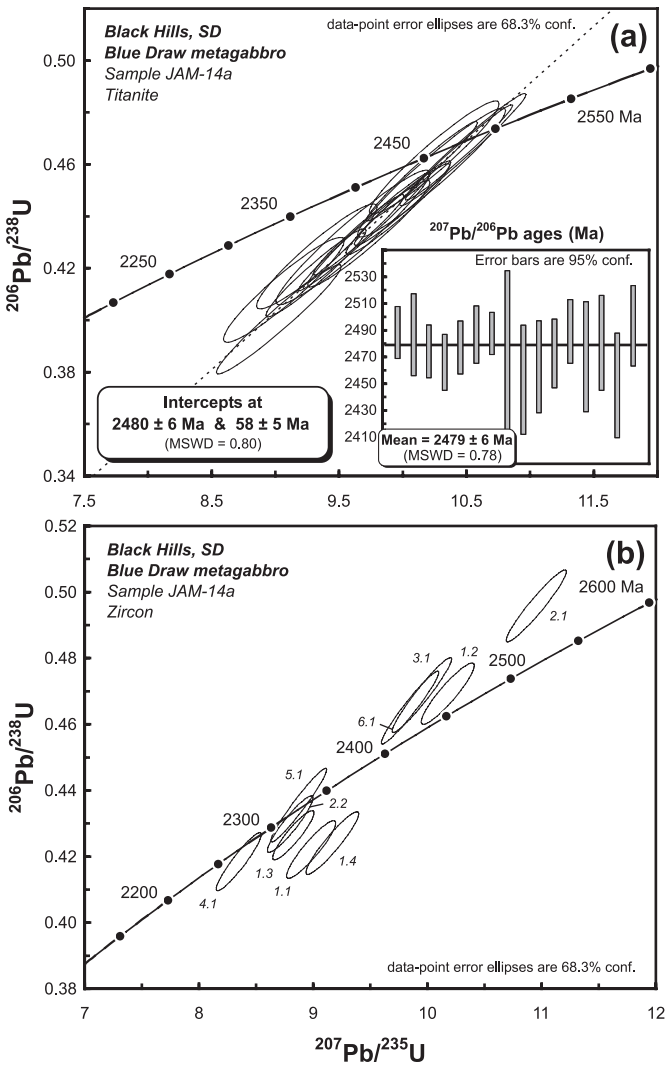

Fig. 4. U–Pb concordia plots of SHRIMP data obtained for titanite and zircon in dioritic pegmatite, sample JAM-14a. (*a*) Plot for titanite (16 spot analyses of two grains, Table 2) in which the upper intercept yields a $^{207}Pb/^{206}Pb$ age of 2480 ± 6 Ma with the lower intercept anchored to the known age of nearby Tertiary intrusions. Free regression of the same data yields upper- and lower-intercept ages of 2484 ± 11 and 215 ± 310 Ma, respectively. Inset (modified after Dahl and McCombs 2005) shows weighted mean $^{207}Pb/^{206}Pb$ age of 2479 ± 6 Ma obtained for the same 16 analyses. All ages reported with 2σ errors. (*b*) Plot for zircon (10 spot analyses of six grains) with data ellipses labeled with grain and spot numbers from Table 2. The data show a pattern of disturbed ages within and among the grains, spread out more or less along concordia, such that an unambiguous upper intercept age cannot be inferred. SD, South Dakota; MSWD, mean square of the weighted deviation; conf., confidence. See text for discussion.

were undertaken to date the host titanite independent of the presumably magmatic zircon inclusions, and thereby to assess whether they were cogenetic or inherited.

Accordingly, a PbSL experiment (method of Frei and Kamber 1995) was first undertaken on a 400 mg separate of purified titanite obtained from pegmatite sample Z-3a in the hope of independently dating both titanite host and zircon inclusions in a single experiment. Isotopic data for six successive leachates of the titanite are summarized in Table 1 and plotted in Fig. 3. Unfortunately, the $^{207}Pb/^{204}Pb$ versus $^{206}Pb/^{204}Pb$ diagram (Fig. 3*a*) shows that the behavior of uranogenic Pb among the leach steps is complicated, thereby yielding no isochron and probably reflecting an age mix of predominant titanite and subordinate zircon. An errorchron based upon all six leach steps in Fig. 3*a* yields an apparent $^{207}Pb/^{206}Pb$ (PbSL) age of 2443 ± 160 Ma (2σ), which represents an imprecise mean age of the titanite and (relatively disturbed) zircon. The $^{208}Pb/^{204}$ Pb versus $^{206}Pb/^{204}Pb$ diagram (Fig. 3*b*) shows similarly complex behavior of thorogenic Pb among the leach steps, in which leach steps 3 and 6 are dominated by a low Th/U phase (probably zircon: Th/U = 0.2–0.7, Table 2), whereas leach steps 4 and 5 reflect the influence of a higher Th/U phase (probably titanite: Th/U = 2.1–6.2, Table 2). Moreover, the higher Th/U trend yields two-point apparent PbSL ages of 2477 ± 4 Ma (leach steps 1 and 4) and 2489 ± 3 Ma (leach steps 1 and 5), which closely approximate the SHRIMP age of the titanite (Fig. 4*a*, described later in the text), whereas the lower Th/U trend as defined by leach steps 1 and 6 yields a two-point apparent PbSL age of 2341 ± 4 Ma that closely approximates the apparent mean SHRIMP age of zircon (Fig. 4*b*, also described later in the text). Thus, the PbSL data are able to discern host titanite from included zircon, whereas the arbitrary two-point isochrons (and others shown in Fig. 3*a*) indicate a much older intrusive age of the BDM than previously recognized. However, because of scatter inherent in the data set (Fig. 3*a*), probably reflecting a contribution from metamict zircon, it was impossible to pinpoint the ages of either titanite or zircon growth in the BDM with confidence using this bulk technique. Consequently, the follow-up SHRIMP spot analyses were undertaken, as described later in the text.

SHRIMP spot-age determinations of the discrete compositional domains noted earlier in the text for the titanite revealed no measurable age difference at the ~30 μm analytical scale (Table 2). In particular, data for eight individual analyses in both grain 1 (Th/U = 2.1–3.0) and grain 2 (Th/U = 4.7–6.2) yield upper-intercept $^{207}Pb/^{206}Pb$ ages of 2487 ± 15 and 2472 ± 22 Ma (2σ), respectively, which are indistinguishable within error (Fig. 4). A precise, weighted mean $^{207}Pb/^{206}Pb$ age of 2479 ± 6 Ma (2σ) is obtained on the basis of all 16 spot analyses (Fig. 4*a*, inset). An upper-intercept age of 2480 ± 6 Ma (2σ) anchored to a lower intercept of 58 ± 5 Ma (age of nearby Tertiary intrusions) is also obtained in Fig. 4*a* by excluding only spot 1.9, which exhibits relatively high common ^{206}Pb (Table 2), whereas free regression of all the data yields comparable upper and lower intercept ages (within error) of 2484 ± 11 and 215 ± 310 Ma, respectively. The Blue Draw gabbro was intruded into cold sedimentary country rock (Redden 1987) and, during subsequent polyphase metamorphism, this suite of rocks never exceeded biotite-grade temperatures (Fig 2; Redden et al. 1990). Assuming a Pb closure temperature for titanite of ~680–700 °C or higher for grains with an effective diffusion radius of 1 mm (Cherniak 1993; Dahl 1997), the titanite ages reported here clearly establish a 2480 Ma intrusive age for the Blue Draw mafic sill. This result contrasts sharply with the previous age estimate for the sill (dated by U–Pb discordant zircon, Redden

Fig. 5. (*a*) Incremental-release spectra of Cl/Ca-, Cl/K-, Ca/K-, and age-derived from Ar-isotopic analysis of hornblende from metadiorite, sample BD-5 (uppermost BDM, Fig. 2). t_{int}, integrated date. (*b*) Plot of Ca/K vs. Cl/K for hornblende in which ratios independently derived from analyses by electron microprobe and mass spectrometer are compared. EMP, electron microprobe; T, temperature. See text for discussion.

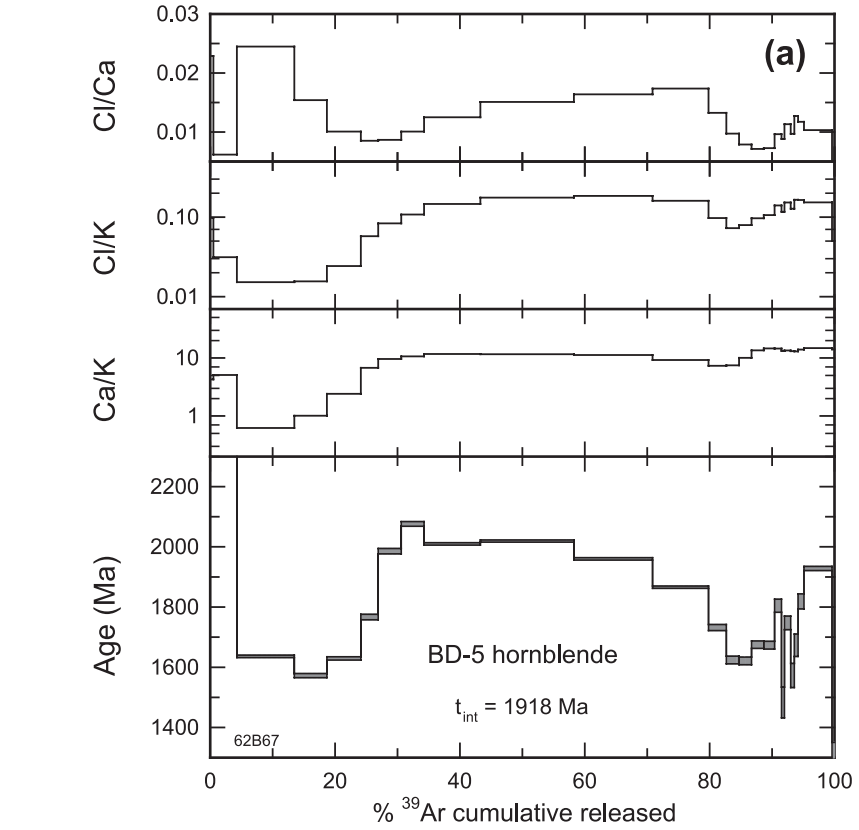

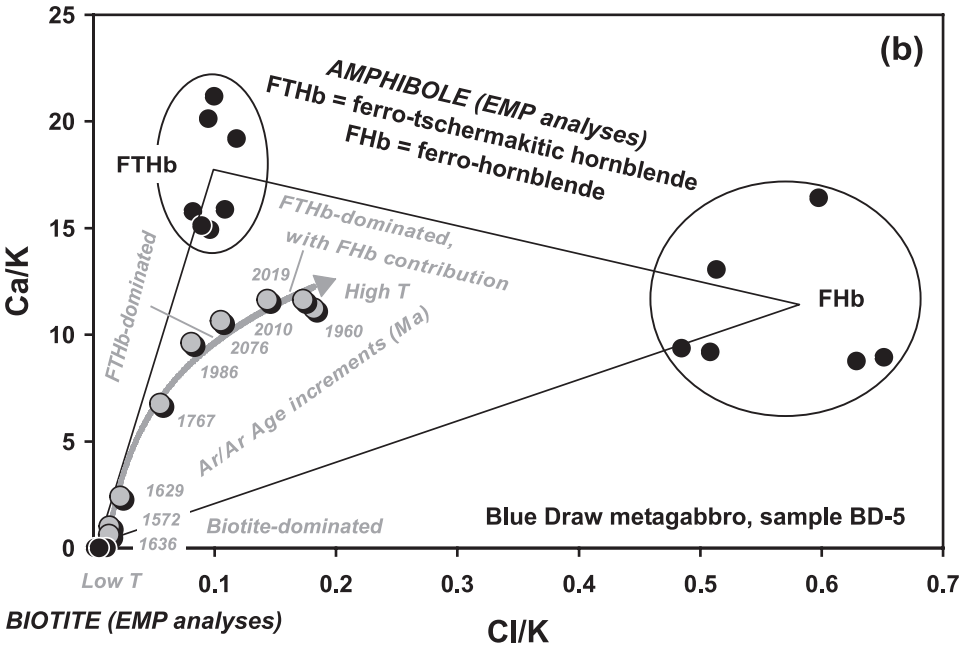

et al. 1990), which suggested that it intruded some 300 million years later.

Zircon

Measured Th/U ratios of 16 spots analyzed within six grains of BDM zircon range from ~0.2–0.7 (Table 2), which coupled with the consistent oscillatory zoning and skeletal morphologies mentioned earlier and the age relationships shown in Fig. 4, support a primary magmatic rather than inherited or metamorphic origin for the zircon. Imaging of zircon from sample JAM-14a reveals that only restricted parts of most grains are non-metamict and therefore suitable for age determination; this likely accounts for the extreme U–Pb discordance encountered in the original thermal ionization mass spectrometry analysis of single-grain separates. However, as illustrated in Fig. 4*b*, even the SHRIMP U–Pb microanalyses of relatively pristine and concordant domains within these zircon grains reveal complex age relationships. Specifically, the individual SHRIMP spots are arrayed as a spread of apparent ages along or near concordia (Table 2, Fig. 4*b*) between 2458 ± 16 and 2284 ± 20 Ma, which is reported here as 2390 ± 70 Ma (an apparent age not dissimilar to the ~2340 Ma bulk date estimated by PbSL methods that are reported earlier in the text). From labeled error ellipses in Fig. 4*b*, it is evident that the spread of apparent-age domains varies both within and between grains. This apparent-age spread is difficult to explain, but may indicate (1) multiple episodes of zircon growth between ~2460 and 2280 Ma, following BDM intrusion at 2480 Ma (Fig. 4*a*); (2) simple age mixing along or near concordia, in which the SHRIMP spots variably straddled end-member growth domains ranging from 2460 to 2280 Ma or from 2460 to 1715 Ma; or (3) differential Pb loss (resetting) among the analyzed zircons, at ~2250 Ma and (or) later.

Possibility (1) is considered unlikely because there is no convincing textural evidence for significant development of new zircon as overgrowths or embayments on older cores. Likewise, good evidence for subsolidus recrystallization is lacking inasmuch as the internal, often oscillatory, zoning is largely not disrupted. Possibility (2) is considered unlikely for the same reasons as stated earlier in the text, although in both cases neocrystallization or recrystallization of zircon cannot be ruled out below the micron-scale of observation. Possibility (3) is considered the most likely explanation, as discussed later in the text, but with preservation of a simple pattern of Pb loss in Fig. 4*b* precluded by the multiplicity of low-grade metamorphic overprints known to have affected the Nemo area from 1820–1715 Ma and perhaps also at ~2250 Ma. In particular, occurrences of polyphase, low-grade monazite in the Nemo area have been dated at ~1820 Ma, 1750 Ma (predominant population), and 1715 Ma (Dahl et al. 2005*a*, 2005*b*). Likewise, the Nemo area may have experienced minor hydrothermal activity during an episode of Tertiary magmatism that was widespread throughout the northern Black Hills (DeWitt et al. 1989). Indeed, the ~60 Ma Vanocker stock crops out extensively just several kilometres north of the map area shown in Fig. 2. Accordingly, a local pattern of disturbed, ~1400–1300 Ma $^{40}Ar/^{39}Ar$ ages of Paleoproterozoic micas between these areas has been interpreted as resulting largely from interaction with Tertiary hydrothermal fluids (Dahl et al. 1999).

In summary, thermal overprinting mainly at ~1750–1715 Ma (coincident with Wyoming–Superior collision and Harney Peak granite emplacement) and (or) ~60 Ma (Tertiary intrusions in the northern Black Hills) is thought to have isotopically disturbed the BDM zircon grains, which are also highly altered and pitted internally. As such, they appear to record minor ancient radiogenic Pb-loss (Fig. 4*b*), in contrast to with the relatively pristine and concordant titanite grains (Fig. 4*a*). The most concordant older zircon spot analyses (Fig. 4*b*) suggest an age near 2430 Ma; this represents a minimum estimate of the true BDM intrusive age in light of the well-defined 2480 Ma age for coexisting titanite that is documented earlier in the text. Finally, despite the scatter evident in Fig. 4*b*, the ~2460–2280 Ma apparent ages of zircon inferred from the SHRIMP analyses (see also Table 2) nevertheless corroborate the 2480 Ma titanite age inasmuch as they also signify an older timeframe of rifting than previously recognized in the easternmost Wyoming craton.

Hornblende

The BD-5 hornblende diorite was sampled from a layer immediately below the dioritic pegmatite layer that yielded the dated titanite megacrysts. The rock was extremely fresh both in outcrop and in thin section. Given the uniformly low grade of the metamorphic overprints, the expectation was that the hornblende would yield a precise age to corroborate the 2480 Ma growth age of the adjacent titanite. Instead, the amphibole separate from BD-5 gave a $^{40}Ar/^{39}Ar$ incremental release spectrum that is highly discordant (Fig. 5*a;* Table 3). This complexity apparently reflects several factors: (1) compositional zonation in the amphibole (verified by electron microprobe), which ranges from an olive green ferro-hornblende in grain cores to a blue–green ferro-tschermakitic hornblende in overgrowths (McCombs 2002); (2) presence of tiny inclusions of mica and feldspar in the amphibole (verified optically); and (3) partial ^{40}Ar loss from the amphibole (and (or) included biotite) during Paleoproterozoic (and (or) Tertiary) reheating events.

The presence of mineralogical heterogeneities in the hornblende is independently indicated in the Ca/K, Cl/K, and Cl/Ca ratios derived from the step heating (Fig. 5*a*). In particular, the lower Ca/K ratios evident in earlier (i.e., relatively low temperature) increments indicate that a portion of the Ar was derived from tiny mica and (or) feldspar inclusions observed optically, whereas the relatively higher Ca/K ratios in later increments indicate that the Ar was mostly derived from the host hornblende itself.

In light of these heterogeneities, the spectrum is a mixed one that can be approximately deconvolved using independently known Ca/K and Cl/K ratios of the host and impurity phases. Fig. 5*b* is a plot of these ratios, as determined by electron microprobe, for mineral reservoirs containing radiogenic argon in BD-5: ferro-hornblende, ferro-tschermakitic hornblende, and biotite that form the apices of a compositional phase triangle. Superimposed in Fig. 5*b* is the trajectory of successive age increments in Ca/K–Cl/K space for BD-5 hornblende, as defined by the Ar-isotopic analysis of individual temperature increments in the step-heating experiment (Table 3, Fig. 5*a*). The plot shows a trend of increasing apparent age from ~1570 to 1635 Ma near the biotite apex up to ~1985–2075 Ma in the higher-temperature increments.

The low-temperature steps are dominated by degassing of biotite, whereas the higher-temperature steps appear to reflect progressive degassing of mostly the older amphibole. The curved trajectory further suggests that the ferro-tschermakitic hornblende (low Cl/Ca ratio) began to degas at somewhat lower temperature than the ferro-hornblende (higher Cl/Ca ratio; cf. Figs. 5*a*, 5*b*).

The three oldest age increments in the two-tiered $^{40}Ar/^{39}Ar$ spectrum are 2076 ± 16, 2010 ± 8, and 2019 ± 8 Ma (all ±2σ), which correspond to degassing temperatures of 1010, 1020, and 1030 °C, respectively. Ratios of Ca/K and Cl/K for the last two of these steps plot within error along the two-amphibole compositional join defined by the electron microprobe analyses, indicating that the Ar that degassed in these steps corresponds to hornblende mainly, with either minor or no biotite. Thus, the minimum age of hornblende growth is apparently ~2010 Ma, whereas a weighted mean date of 2050 ± 50 Ma (±2σ) is obtained from the five highest-temperature increments (Table 3; Figs. 5*a*, 5*b*). By similar reasoning, the three youngest apparent-age increments of 1636 ± 4, 1572 ± 7, and 1629 ± 5 Ma, which represent degassing of argon at 850, 900, and 940 °C, respectively (Table 3), correspond to maximum apparent age of biotite with minor or no hornblende contribution. This inference follows from the fact that the Ca/K and Cl/K ratios of the first two of these degassing steps correspond closely to those ratios as independently determined by electron microprobe (Figs. 5*a*, 5*b*). The ~2010 Ma hornblende and ~1635 Ma biotite dates cannot be interpreted as cooling ages because fast cooling of the BDM against cold sedimentary country rock would have been manifested as ~2480 Ma mineral dates, which are not observed. Instead, and without independent evidence for thermal events at ~2010 or ~1635 Ma, the hornblende and biotite dates are interpreted as mixed ages that resulted from differential resetting at ~2250(?), ~1820–1715 and (or) ~60 Ma. These respective dates correspond to inferred and known times of reheating in the Nemo area.

Summary

The upper BDM yields the following sequence of apparent ages: titanite (2480 Ma) > zircon (~2460–2280 Ma) > hornblende (~2075–1985 Ma) > biotite (~1635 Ma). Taken together, this ~2480–1635 Ma apparent-age spread is likely the result of differential isotopic resetting that occurred in response to multiple episodes of Paleoproterozoic, low-grade thermotectonic activity well documented in the Nemo area. Specifically, titanite in the BDM was undisturbed, whereas coexisting zircon, hornblende, and biotite were progressively more reset. In the country rocks intruded by the BDM, biotite and muscovite exhibit even younger $^{40}Ar/^{39}Ar$ dates, ranging from ~1460–1300 Ma (Dahl et al. 1999), which are interpreted as evidence of additional partial resetting by Tertiary hydrothermal activity. In conclusion, because of the variably disturbed mineral-isotopic systems in the BDM sill and adjacent Nemo country rocks, only the SHRIMP analyses of titanite (Table 2; Fig. 4*a*) are interpreted to establish a robust age of intrusion for the sill, at 2480 ± 6 Ma.

Discussion

Our new age for intrusion of the BDM constrains a significantly older timeframe of Paleoproterozoic sedimentation and rifting in the Black Hills than was previously recognized (legend, Fig. 2), as well as a greater extent of missing rock record than was previously recognized across the EU. This result also has important implications for the history of regional tectonism and of continental assembly and dispersal, as developed later in the text.

Paleoproterozoic synthesis (northern Black Hills)

The older rift sequence exposed at Nemo and environs (Fig. 2; Redden et al. 1990) was deposited between 2559 ± 6 Ma (crystallization age of the LEG, McCombs et al. 2004) and 2480 ± 6 Ma (intrusive age of the BDM, Fig. 3*a*). Moreover, the presence of detrital pyrite (± chromite?) in fuchsitic horizons of the Boxelder Creek quartzite indicates that an ultramafic source (no longer exposed) was exposed from 2560–2480 Ma, whereas the presence of LEG clasts in the basal quartzite indicates that the LEG was another exposed source during this timeframe. Further, a 2560–2480 Ma depositional timeframe for the Benchmark Iron Formation indicates that it significantly predated the atmosphetic oxygenation event that triggered iron formation deposition worldwide (Barley et al. 2005), whereas deposition of the ~2000 Ma Homestake Iron Formation clearly postdated this event. The stratigraphically much older Nemo Iron Formation is considered part of the Neoarchean metasedimentary suite that includes the paragneissic component of the BFG (DeWitt et al. 1986, 1989; Redden et al. 1990), and as such may have been deposited between ~2900? and 2600 Ma (legend, Fig. 2).

The EU (Fig. 2) separates the overlying Estes metaconglomerate from the underlying Benchmark Iron Formation. The accepted depositional model for Estes sedimentation is one of regional rifting, development of growth faults, and infilling of fault-block basins with conglomeratic sediments of local origin (Redden 1987). Deposition of the Benchmark Iron Formation occurred prior to 2480 Ma, as noted above, whereas carbonate horizons in the overlying Estes and Roberts Draw Formations were deposited after ~2100 Ma, and possibly as late as ~2015 Ma, on the basis of chemostratigraphic (i.e., carbon isotopic) and lithostratigraphic correlations with the Upper Nash Fork Formation of southeastern Wyoming (Bekker and Eriksson 2003; Bekker et al. 2003; Dahl and McCombs 2005). Thus, the EU potentially represents a hiatus of between ~380 and 465 Ma. Regionally, a more complete record of ~2450–2015 Ma sedimentation is preserved in the Snowy Pass supergroup, southeastern Wyoming, that includes three horizons of glacial diamictites that are stratigraphically older than the Nash Fork Formation but notably absent in the Nemo area. Deposition of the Snowy Pass, Huronian, and correlative diamictites worldwide (Paleoproterozoic Snowball Earth) is independently dated at ~2320–2220 Ma (Bekker et al. 2003; Hilburn et al. 2005; Barley et al. 2005). Therefore, the conspicuous absence of diamictite in the Nemo sequence is potentially explained by an episode of geon 21 erosion (i.e., the ~2200?–2100? Ma EU; see Fig. 2 immediately preceding deposition of the Estes conglomerate.

Above the Estes unconformity, occurrences of the ~2100–2015 Ma Estes metaconglomerate and the 1974 ± 8 Ma protolith of the Gingrass Draw slate (equivalent to Ellison Formation tuffs in the Lead–Deadwood area; dated by U–Pb zircon, Redden et al. 1990) effectively bracket deposition of

the intervening units. That is, protoliths of the Roberts Draw marble, the overlying metabasalt (equivalent to the Poorman Formation in the Lead–Deadwood area), and the overlying meta-iron formation (equivalent to the Homestake Formation in the Lead–Deadwood area) are all considered to be ~2015–1975 Ma in age. Listric growth faults in the Nemo area (Redden 1987) truncate the older EU and are associated with deposition of Estes conglomerate; one such fault can be seen juxtaposing Estes conglomerate and Boxelder Creek quartzite just west of the Nemo area (Fig. 2). Available evidence suggests that the southeast margin of the Wyoming craton was undergoing active rifting at about the same time, at 2092 ± 9 Ma (metagabbro plug, Premo and Van Schmus 1989) and 2011 ± 1.2 Ma (Kennedy dyke swarm, Cox et al. 2000). Thus, both listric normal faulting at ~2100–2015 Ma in the Nemo area and ~2015–1975 Ma deposition of Poorman mafic volcanics and the Homestake Iron Formation in the Lead–Deadwood area are interpreted to have occurred in response to regional lithospheric extension in the Black Hills between ~2100 and 1975 Ma.

The deformational events responsible for pre-EU folding in the Nemo area and post-EU overturning to the southeast (Fig. 2) are cryptic in both nature and timing. Redden (1987) postulated an early episode of approximately east–west compression accompanied by metamorphism to account for pre-EU folding, which he inferred from mapped erosional relief along the unconformity (Fig. 2). Given the protracted period postulated for rifting (380–465 Ma) and the possibility of two periods of mafic magmatism at 2480 and ~2000 Ma, it is perhaps more likely that an intervening compressional event caused both the pre-EU folding and the geon 21 erosion associated with the unconformity. Following this scenario, the ancient Pb loss inferred in the BDM zircon may have occurred primarily at ~2250–2200 Ma, during early metamorphism and fabric development associated with pre-EU folding, as interpreted from the trajectory of zircon data points observed along or near concordia (Fig. 4*b*). Subsequent metamorphism associated with 1820–1715 Ma compression and later hydrothermal activity at 60 Ma, both noted earlier in the text, may have facilitated additional but minor Pb loss, thereby obscuring this older trajectory. Alternatively, Redden (1987) considered a less likely hypothesis that the steep northwest plunges of all lineations and the northwest trends of all axial planar foliations in the Nemo area could have resulted solely from the known post-EU folding and metamorphism, which is dated at 1750–1715 Ma (Paleoproterozoic D_2; Dahl et al. 2005*a*, 2005*b*). This hypothesis is considered further unlikely inasmuch as it fails to account for the apparent ~2460–2280 Ma trajectory defined by the BDM zircon data (Fig. 4*b*). More data are needed to test these two possibilities.

All of the units in the Nemo area were structurally overturned to the southeast, on a approximately northeast-trending axis (modern coordinates; Woo 1952; Redden et al. 1990). Redden (1987) considered this late overturning to be related to the NE-trending nappe and thrusting event (Paleoproterozoic D_1) known elsewhere in the Black Hills. Recent evidence relates these structures to approximately northwest-directed accretion of the northern Yavapai island-arc terrane from the south (inset, Fig. 1), at ~1770–1780 Ma (Dahl et al. 1999, 2005*a*, 2005*b*). Thus, the overturning event in Nemo and environs likely formed at ~1770–1780 Ma, just prior to the onset of latest approximately east–west folding at 1750 ± 10 Ma.

Strengthening the pre-2480 Ma Wyoming–Superior connection

The location of the Wyoming craton in a late Neoarchean supercontinent is the subject of active debate. The main "piercing point" proposed in the original Kenorland reconstruction was the Paleoproterozoic rift- to passive-margin sequences exposed in southeastern Wyoming (Snowy Pass supergroup) and southern Ontario (Huronian supergroup), which Roscoe and Card (1993) envisioned as once comprising a common depocenter (Fig. 6*a*). Although supported by subsequent paleomagnetic and geochronologic data (Harlan et al. 2003*a*), the non-unique characteristics of the two supergroups and the previously poor geochronologic resolution of presumed Black Hills equivalent rocks requires more rigorous testing of their proposed reconstruction. In this regard, the narrowed 2560–2480 Ma depositional timeframe for the older sedimentary rift succession in the Black Hills (cf. ~2560–2170 Ma prior to this study; Redden et al. 1990) strengthens stratigraphic correlation of the Boxelder Creek sandstone (Nemo, South Dakota) and the ~2450 Ma Magnolia sandstone (Snowy Pass supergroup, southeastern Wyoming: Aspler and Chiarenzelli 1998; Bekker and Eriksson 2003; Bekker et al. 2003). Moreover, the revised, older age of the Boxelder Creek sandstone also aligns it temporally with the Livingstone Creek sandstone of the Huronian supergroup (southern Ontario, Fig. 6*a*), which is cut by 2480–2490 Ma mafic-layered plutons of the EBL intrusive suite (James et al. 2002). Thus, the near-synchroneity of basal rift-basin sedimentation in southeastern Wyoming, southern Ontario, and the Black Hills is consistent with the existence of a single epicratonic basin of facing rift margins at 2500–2450 Ma.

Continental rifting is commonly manifested in the emplacement of mafic igneous rocks on either side of the rift margins. For instance,the southern Superior craton contains extensive mafic rocks intruded at ~2490–2445 Ma (Matachewan dykes and EBL), 2217–2216 Ma (Nipissing–Senneterre sills and dykes), 2172–2167 Ma (Biscotasing dykes), 2125–2101 Ma (Marathon dykes), and 2077–2076 Ma (Fort Frances dykes), consistent with rifting or lithospheric extension during these times (Ernst and Buchan 2001; Hamilton et al. 2002). Elements of these stages at selected times are presented schematically as "snapshots" in Figs. 6*a*–6*c*. In the earliest stage of this sequence, the older, 2473^{+17}_{-9} Ma component of the voluminous Matachewan mafic dyke swarm (Heaman 1997) and the 2490–2475 Ma mafic components of the EBL intrusive suite (James et al. 2002) intruded the south-central part and southern margin, respectively, of the Superior craton (Fig. 6*a*). However, a longstanding obstacle to linking the Wyoming craton to the southern Superior Province in the earliest Paleoproterozoic, as considered earlier in the text, has been the apparent lack of rift-related rocks of 2500–2450 Ma age in the eastern Wyoming craton (Dahl et al. 1999; Harlan 2005). Significantly, the refined U–Pb age for the BDM documented in this study probably indicates that the easternmost Wyoming lithosphere was still undergoing extension or rifting as late as 2480 Ma, simultaneous with emplacement of a 250 km long belt of mafic-layered intru-

sions extending east-northeast through Sudbury, Ontario (Fig. 6*a*). Moreover, the EBL intrusive suite aligns spatially with the BDM if the Superior and Wyoming cratons are restored to the Kenorland configuration proposed by Roscoe and Card (1993). This alignment of shallow-crustal, mafic plutonic rocks of identical age intruded into previously undeformed sedimentary rocks considerably strengthens the "piercing point" linking the Wyoming craton to southern Superior in a Kenorland fit (Fig. 6*a*).

The Biscotasing, Marathon, and Fort Frances (or "Kenora–Kabetogama", including the 2067 ± 1 Ma "Franklin" dyke of Schmitz et al. 2006) swarms likely reflect episodic plume or hotspot activity centered south of the Superior craton and east of the MRV terrane (Buchan et al. 1993, 1996; Ernst and Buchan 1993, 2001; Schmitz et al. 2006). This hypothesis agrees with the one first proposed by Southwick and Day (1983), who suggested that the radiating Fort Frances diabase swarm could have been injected laterally from the southeast to the northwest from a hotspot centered beneath the future site of the Animikie Basin. Consequently, Figs. 6*a*–6*c* imply that the pattern of magmatism from ~2480 to 2000 Ma in the southern Superior craton and parts of the Wyoming craton could be a consequence of progressive, relative motion of the rifting supercontinent over a single, very long-lived plume or hotspot. Recent studies by Buchan et al. (2000) and Hamilton et al. (2002) have shown that the latitudinal drift and azimuthal orientation of the Superior craton during the early to middle Paleoproterozoic are very tightly constrained. These authors used reliable, "key" paleomagnetic pole data (i.e., demonstrated primary remanence on precise U–Pb-dated mafic dykes and sills) to reveal that although the Superior craton occupied low latitudes at 2450 Ma it may have undergone more than 50° of latitudinal drift and almost 90° of net counterclockwise rotation by ~2170 Ma. Between 2170 and 2075 Ma, the craton drifted back towards lower latitudes by some 15°, at first going through nearly 45° of counterclockwise rotation and then about 12° of clockwise rotation. With these considerable cratonic excursions, therefore, it is difficult to imagine a single, long-lived plume and lithosphere interaction. Rather, we favor a scenario in which a drifting Superior craton or amalgamated supercontinent precursor (Kenorland) periodically intersected upwelling plumes for shorter (<10 Ma) or longer (20–40 Ma) intervals during which mantle-derived gabbroic melts were transferred to the crust.

Figure 6*b* shows that, at 2170 Ma, much of the southern and eastern Superior craton was bisected by the extensive (>300 000 km^2) Biscotasing diabase swarm (Buchan et al. 1993; Halls and Davis 2004). On the presumed opposite side of this rift margin, in the south-central Wyoming craton (present-day coordinates), this swarm is ostensibly matched by a 2170 ± 8 Ma quartz diorite dyke that cuts Archean supracrustal units in the southern Wind River Range of Wyoming (Harlan et al. 2003*a*). Paleomagnetic study of this dyke led Harlan et al. (2003*a*) to conclude that a closest-approach fit constrained by paleolatitude is permissive of the Wyoming–Superior craton reconstruction proposed by Roscoe and Card (1993). The fit shown in Fig. 6*b* is similar to this closest-approach fit, but it implies some separation and clockwise rotation of the Wyoming craton after 2450 Ma. The Marathon diabase dykes define a broad, north-trending swarm north of Lake Superior and have been dated precisely as a series of brief, episodic magmatic pulses intruding the south-central Superior Province between 2121 and 2101 Ma (Buchan et al. 1996; Hamilton et al. 2002; Davis and Stott 2003). Figure 6*c* shows a possible temporal equivalent (within analytical error) of this mafic magmatism in the southern Wyoming craton—a metagabbro plug that intruded clastic sediments (Cascade quartzite) of the lower Snowy Pass supergroup in the Sierra Madre Range, at 2092 ± 9 Ma (Premo and Van Schmus 1989). Because of a lack of primary paleomagnetic poles from the Wyoming craton at this time (~2100 Ma), the degree of relative clockwise rotation of Wyoming away from Superior is not constrained. However, the amount of azimuthal drift shown in Fig. 6*c* is consistent with the spatial distribution of mafic, hotspot-fed magmatism on both cratons at 2125–2090 Ma. Moreover, repeated dyke swarm magmatism at 2077–2067 Ma (Fort Frances – Franklin dykes; Wirth et al. 1995; Buchan et al. 1996; Schmitz et al. 2006) and 2011 ± 1 Ma (Kennedy dykes, Cox et al. 2000) is also consistent with this geometry (Fig. 6*c*).

Fit of the Superior and Wyoming cratons at 2480–2450 Ma may also be assessed using the recent configuration for supercraton Superia (Bleeker 2003, 2004; Bleeker and Ernst 2006), and is shown in Fig. 6*d*. These authors have proposed, on the basis of possible 2450 Ma dyke correlation and similarities in basement-cover sequence geology, that the Hearne craton may have occupied a position abutting the (present-day) south margin of the Superior craton adjacent to Karelia (dashed outline, Fig. 6*d*). In this reconstruction, the Wyoming craton was speculated to have occupied a wide re-entrant west of the Hearne and south of the Superior cratons. However, using the same relative Wyoming–Superior orientation as in the modified Roscoe and Card (Kenorland) reconstruction, we note that an excellent fit is made with a triple junction formed between Superior–Wyoming and a third cratonic fragment identified by Bleeker and Ernst (2006) to be Karelia. This relationship is significant irrespective of whether the Wyoming craton was immediately adjacent to Karelia, as we propose, or whether the Hearne craton was intervening (Bleeker 2004; Bleeker and Ernst 2006).

Evident from the possible paleocontinental fits shown in Figs. 6*a* and 6*d* is the principal conclusion that the reconstructions of Roscoe and Card (1993) and Bleeker and Ernst (2006) are mutually incompatible. There is inadequate space and insufficient rotational freedom in the Hearne craton paleomagnetic data set (~2450 Ma Kaminak dykes, summarized in Bleeker 2004) for this craton to have occupied the apparent re-entrant between the Wyoming craton and the MRV region of the Superior craton (Fig. 6*d*). Likewise, the Wyoming craton cannot be accommodated easily in a space west of a Hearne–Karelia amalgamation and south of the Superior craton (present-day coordinates). The primary paleopole data for Karelia at 2450 Ma is incompletely understood, but nonetheless it suggests that this craton did not occupy the position shown in Fig. 6*d* (Mertanen et al. 1999; Pesonen et al. 2003). However, any space thereby liberated by Karelia cannot simply be replaced by the Hearne craton because the paleomagnetic data for the latter again constrain any rotations to have been far smaller than required. Therefore, it appears that there

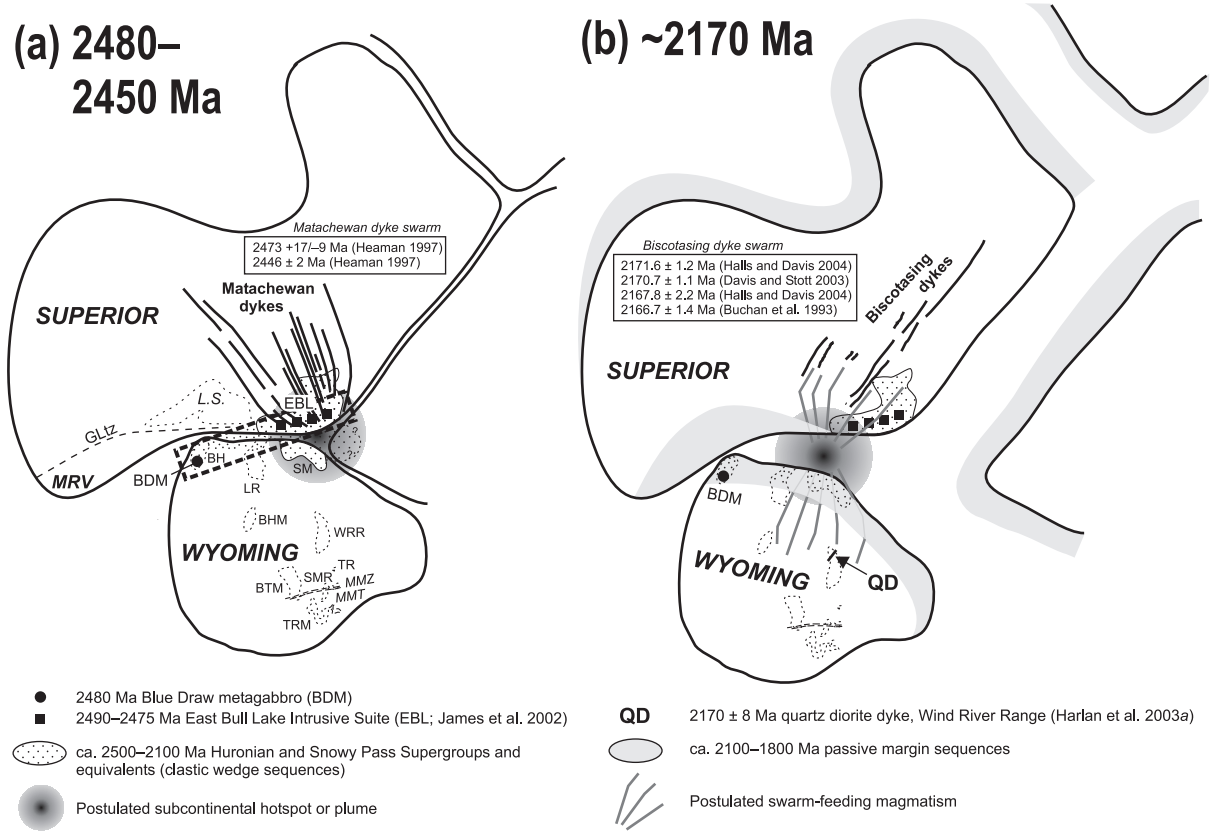

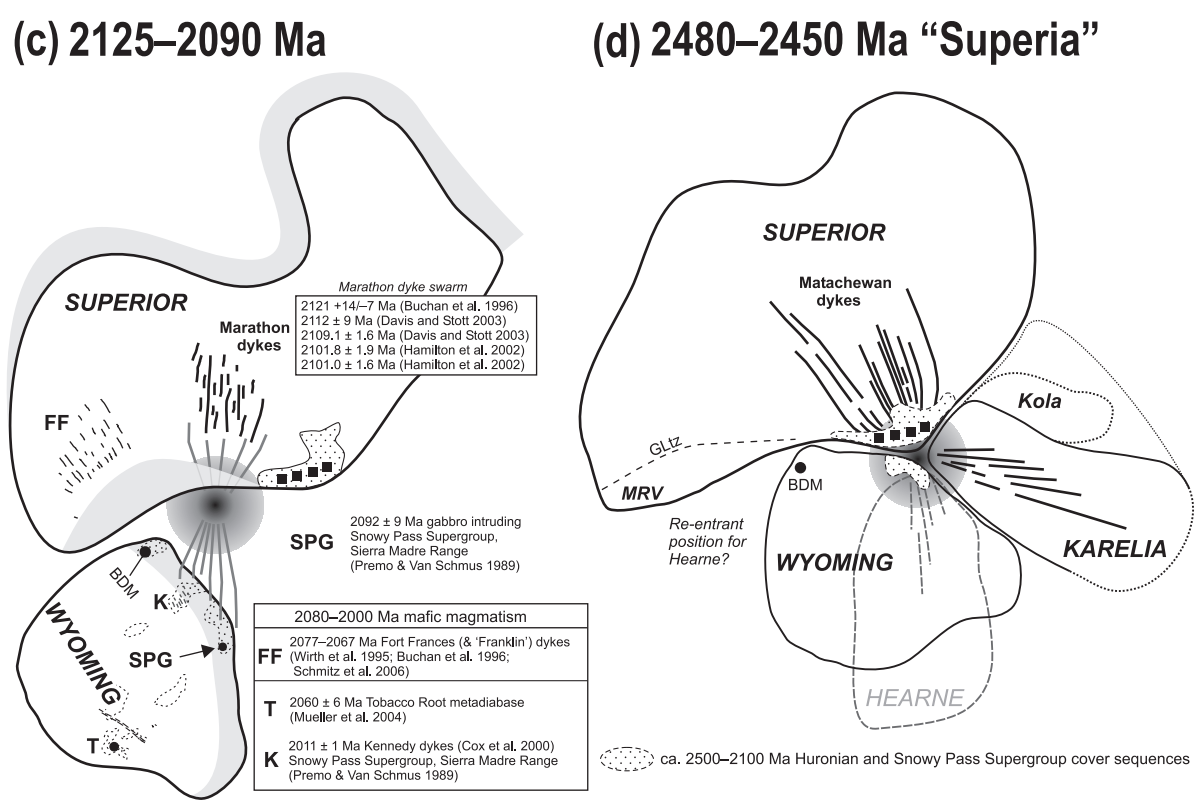

Fig. 6. Final assembly of supercontinent Kenorland, showing cratonic elements amalgamated by ~2600–2550 Ma, with juxtaposition of the southern Superior (with Minnesota River Valley terrane, MRV) and eastern Wyoming cratons, and its subsequent dispersal between ~2500 and 2100 Ma (modified after Williams et al. 1991; Roscoe and Card 1993; and Harlan et al. 2003*a*). (*a*) Principal igneous activity affecting the Superior craton between ~2480 and 2450 Ma includes the giant radiating swarm of 2473–2446 Ma Matachewan diabase dykes and the 2490–2475 Ma mafic-layered intrusions of the East Bull Lake suite (EBL), whereas in the eastern Wyoming craton the 2480 Ma Blue Draw metagabbro (BDM) intrudes the Black Hills (BH). A possible plume source for the mafic magmatism (dimensions of plume head schematic only), as well as clastic sedimentary prisms deposited in incipient rifting basins, are also shown. GLtz, Great Lakes tectonic zone; L.S., Lake Superior; BHM, Bighorn Mountains; BTM, Beartooth Mountains; LR, Laramie Range; SMR, Sierra Madre Range; TR, Teton Range; TRM, Tobacco Root Mountains; MMT, Montana metasedimentary terrane; MMZ, Madison mylonite zone (Erslev and Sutter 1990); WRR, Wind River Range. (*b*) The ~2170 Ma intrusive events that affected the Superior craton (2172–2167 Ma Biscotasing dyke swarm) and their temporal equivalent in the Wyoming craton (2170 ± 8 Ma quartz diorite dyke (QD)) are illustrated. Approximate possible position for Wyoming craton, as partly constrained by paleomagnetic data of Harlan et al. (2003*a*) and by QD dyke orientation. BDM, Blue Draw metagabbro. (*c*) 2125–2090 Ma mafic magmatic events affecting Superior (2125–2101 Ma Marathon dyke swarm) and Wyoming (2092 ± 9 Ma gabbro intruding Snowy Pass supergroup (SPG)) cratons. Subsequent magmatism in Superior craton at 2077–2067 Ma (radiating Fort Frances dyke swarm (FF), and in Wyoming craton at 2060 ± 6 Ma (Tobacco Root Mountains, metadiabase (T)) and 2011 ± 1 Ma (Laramie Range, Kennedy dyke swarm, (K)) are shown for reference. BDM, Blue Draw metagabbro. (*d*) Proposed reconstructions of supercraton Superia, showing Hearne–Superior–Karelia juxtaposition (modified after Bleeker 2003, 2004; Bleeker and Ernst 2006) and alternative Wyoming–Superior–Karelia juxtaposition (this study). MRV, Minnesota River Valley terrane; GLtz, Great Lakes tectonic zone; BDM, Blue Draw metagabbro. See text for discussion.

was insufficient space to have accommodated both the Wyoming and Hearne cratons around the south margin of Superior craton in the modified Superia fit suggested here (Fig. 6*d*).

We conclude that the corridor of layered mafic intrusions from Sudbury to Nemo (dashed rectangle, Fig. 6*a*) represents a single axial rift zone along which Superior began to separate from Wyoming during the incipient breakup of Kenorland or Superia at ~2480 Ma. Following this model, Wyoming–Superior separation was complete by ~2100 Ma or shortly thereafter, as evidenced by the younger dykes noted earlier in the text in both cratons. In this context, the ~2250 Ma episode of folding and low-grade thermotectonism inferred in the lower Nemo sequence (this study) and ~2300–2220 Ma compression documented in the upper Huronian sequence (soft-sediment deformation; Shaw et al. 1999), considered together, may have resulted from intervening recollision of the Wyoming and Superior cratons. Finally, between ~2100 and 1865 Ma, the Wyoming craton appears to have remained adrift in a westward direction (modern coordinates, relative to Superior) until it began to dock with Superior again at ~1865 Ma, as part of Laurentia.

Another important problem raised by a pre-2480 Ma Wyoming–Superior connection regards the differences in the Archean geology between the Wyoming craton and the MRV terrane (Frost 1993; and others), which are adjacent to each other in the reconstruction (Fig. 6). Although the MRV and Wyoming cratons have similar cratonization ages, they show very different Pb isotopic enrichments (Wooden and Mueller 1988), suggesting different origins. However, this difference does not preclude their spatial association in the late Neoarchean. Instead, it may suggest that they represent separate exotic Archean fragments that docked with the newly formed greenstone–granite terranes of the Superior cration, along the Great Lakes tectonic zone (GLtz, Fig. 6; Sims et al. 1980) at ~2600 Ma, i.e., immediately following ~2680 Ma cratonization of the Superior Province. Thus, it is perhaps more important to compare the timing and nature of overprinting effects on the margins of ancient cratons when considering their possible spatial associations. For instance, does the eastern Wyoming Province show a late Neoarchean overprint similar to that seen in the Archean rocks preserved south of the Great Lakes tectonic zone along the southern Superior Province?

In southern Minnesota and northern Michigan, ~2600 Ma convergent tectonics accounts for the generation of syntectonic granitoids of this age associated with juxtaposition of the Mesoarchean gneissic blocks (i.e., MRV) and the Wawa greenstone–granite subprovince (Southwick and Chandler 1996; Tinkham and Marshak 2004; Holm et al. 2005; Bickford et al. 2006; Schmitz et al. 2006). Likewise, ~2600–2560 Ma convergent tectonics in the easternmost Wyoming Province accounts for production of 2595 ± 11 and 2559 ± 6 Ma quartzofeldspathic orthogneisses in the Black Hills basement complex (Gosselin et al. 1988; McCombs et al. 2004). Identical age rocks of the same lithology (i.e., the 2557 Ma McGrath gneiss in east-central Minnesota and the 2559 Ma Little Elk (gneissic) granite in the northern Black Hills) are juxtaposed, using the reconstruction of Wyoming first proposed by Roscoe and Card (1993) and compensating for the effects of ~1100 Ma mid-continent rifting. We speculate that the Neoarchean S_1–S_2 fabrics in the northern Black Hills may have formed during this docking event. Conceivably, the Neoarchean S_1 fabric (2595(?) Ma) could have developed when the eastern Wyoming craton collided with the southern Superior craton, and S_2 (2559 Ma) could have formed when this part of the Wyoming craton docked with the MRV. This speculative scenario is embodied in the ~2600 Ma north-pointing arrows shown in Fig. 2, which restores the hypothetical pre-2500 Ma orientation of the Wyoming craton in the Kenorland–Superia configurations (i.e., prior to 120°–140° clockwise rotation between ~2100 and 1850 Ma).

Interestingly, convergence and (or) terrane collision at ~2570–2550 Ma appears to have occurred along almost all inferred margins of the Wyoming craton (inset, Fig. 1; Fig. 6). The presence of 2550 Ma granitoids in the southern Wyoming craton and in the Teton Range (northwest Wyoming) are

thought to be convergence-related (Frost et al. 1998). Also, in SW Montana, 2570–2550 Ma crustal shortening has been inferred in the South Madison Range (Loehn et al. 2004) and in the NW Beartooth Mountains (Pine Creek nappe complex; Mogk et al. 1992), along the NE-trending Madison mylonite zone (MMZ, Fig. 6; Erslev and Sutter 1990) and its possible NE extension, respectively. This episode of shortening is interpreted as representing juxtaposition of the Montana metasedimentary terrane (MMT) with the NW Wyoming craton (Fig. 6; see also Mogk et al. 1992). Thus, the collision of the eastern Wyoming craton (Black Hills), perhaps with southern Superior, the convergence of southern Wyoming, perhaps with Karelia, and the juxtaposition of the Montana metasedimentary terrane with northwest Wyoming may have been synchronous events occurring during the waning stages of Kenorland–Superia growth (Figs. 6*a*, 6*d*). Approximately 800 million years later, this cycle of synchronous convergence and collision at Wyoming cratonic margins was repeated, this time with Wyoming being welded to the Medicine Hat block and Superior craton as part of Laurentia (inset, Fig. 1) between 1865 and 1715 Ma. During this re-docking of the Wyoming craton, terminal thermotectonism peaked at 1770–1760 Ma along its northwestern margin, in southwest Montana (high-grade metamorphism, Mueller et al. 2004; posttectonic magmatism, Jones et al. 2004), and at 1750–1715 Ma along its opposite margins in southeastern Wyoming and the Black Hills (Chamberlain 1998; Dahl and Frei 1998; Dahl et al. 1999, 2005*a*, 2005*b*).

Conclusions

The main focus of this paper has been to document the ~2500–2000 Ma history of rifting along the inferred trailing edge of the Wyoming craton, as depicted in discrete time increments in Figs. 6*a*–6*d*. Yet, Fig. 6 shows neither the ~2500–2000 Ma history of thermotectonism associated with the leading edge of the drifting Wyoming craton nor other Archean blocks (known or presumed) that may have been associated with its northern and western margins during that timeframe. This section addresses several points of interest regarding the Wyoming craton's presumed leading edge.

For example, not shown in Fig. 6 is the Sask craton (Ansdell 2005), in which Archean basement rocks exhibit signatures of Pb isotopic enrichment and ~2500–2440 Ma thermotectonic overprinting (Bickford et al. 2005; Rayner et al. 2005). On the basis of these correlations, Bickford et al. (2005) proposed that the Sask craton may represent a ~2500–2440 Ma rift fragment of an exotic source such as the Wyoming craton, which exhibits similar Pb-isotopic enrichment (Mueller and Wooden 1988), although precisely which margin of the Wyoming craton may have been involved is unspecified. What is known, however, is that between ~2100 and 1770 Ma the Sask craton drifted relatively to the north of the Wyoming craton (modern coordinates) to reach its present position within Laurentia (Manitoba and Saskatchewan, Ansdell 2005). Thus, the paleogeographic relationships shown in Fig. 6 permit speculation that the Sask craton could have originated from either the northern or western margin of the Wyoming craton (present coordinates), which presumably was drifting westward relative to Superior between ~2100 and 1865 Ma (inset, Fig. 1; Fig. 6*c*). The presence of a 2060 ± 6 Ma mafic dyke in southwest Montana (Brady et al. 2004; Mueller et al. 2004), as shown in Fig. 6*c*, might be interpreted in terms of breakup-related magmatism at this time and thus is supportive of this scenario. On the other hand, the Dakota block (Baird et al. 1996; Nabelek et al. 2001; Dahl et al. 2005*b*)—a discrete block of presumed Archean age currently situated between the Wyoming and Superior cratons (not shown in Fig. 6 but see inset, Fig. 1)—represents a discrete exotic fragment and possibly the southern extension of the Sask craton. Accordingly, the Sask craton may have been rifted from the eastern Wyoming craton at ~2100–2000 Ma and drifted relatively northward beginning at this time. In summary, the 2480–2000 Ma positions of the Sask craton and Dakota block, as well as their possible lithotectonic equivalence to each other and to rocks of the Wyoming craton margins, remain as open questions for future study.

The leading edge of the Wyoming craton also experienced major thermotectonism synchronous with the incipient rifting proposed in this study along its trailing edge (Figs. 2, 4*a*, 6). For example, in the Tobacco Root Mountains of southwest Montana (Fig. 6), ~2500–2450 Ma reworking of Archean rocks and subordinate juvenile rocks of this age are well expressed by U–Pb ages of zircon and monazite, whereas the 2060 ± 6 Ma mafic dyke noted earlier in the text (Mueller et al. 1996, 2004; Brady et al. 2004) crosscuts an older (~2500–2450 Ma) deformational fabric of uncertain origin (Roberts et al. 2002; Dahl and Hamilton 2002; Cheney et al. 2004). Moreover, the adjacent South Madison Range (Fig. 6) and other nearby Laramide uplifts preserve similar evidence of ~2500–2450 Ma reworking and subordinate juvenile rocks (Kellogg et al. 2003; Jones et al. 2004; Loehn et al. 2004), indicating that the thermotectonism during this timeframe was not just localized but regionally widespread (Foster et al. 2006).

Finally, the presence of 780 Ma mafic igneous rocks along the western margin of the Laurentia, including the western Wyoming craton (inset, Fig. 1) has been attributed to breakup of the supercontinent Rodinia (Gunbarrel magmatic event, Harlan et al. 2003*b*). Yet, the absence of Grenville-age rocks in these localities implies that the landmass that rifted away from the western Wyoming craton at ~780 Ma was already connected to Wyoming prior to the earlier assembly of Rodinia. Whether this unknown landmass was part of Siberia, Australia, and (or) Antarctica (Sears and Price 2003, and references therein), or was a fragment of the Wyoming craton itself likewise remains as an open question for future study.

Acknowledgments

Andrey Bekker, Wouter Bleeker, Ken Buchan, Mike Easton, Jack Redden, and Bob Wintsch are thanked for useful discussions. Jack Redden also guided us in the field and kindly provided sample Z-3a for our use. Fritz Hubacher and Jeffrey Linder, who received support from NSF grants EAR-0137546 and EAR-0452220 (awarded to K.A. Foland.), are thanked for laboratory help that facilitated the Ar research. Thanks are due also to Chusi Li for his supervision of the electron microprobe analysis. Insightful reviews by Pat Bickford, Louise Corriveau, Ed Duke, and Carol Frost improved the original manuscript significantly, and editorial handling of

the manuscript by Louise Corriveau and guest editor Carol Frost is gratefully acknowledged. This research was funded by NSF grants EAR-9909433 and EAR-0106987 (awarded to P.S. Dahl), and EAR-0107054 and EAR-0137546 (awarded to K.A. Foland), which are also gratefully acknowledged.

References

Aleinikoff, J.N., Wintsch, R.P., Fanning, C.M., and Dorais, M.J. 2002. U–Pb geochronology of zircon and polygenetic titanite from the Glastonbury Complex, Connecticut, USA: an integrated SEM, EMPA, TIMS, and SHRIMP study. Chemical Geology, **188**: 125–147.

Ansdell, K.M. 2005. Tectonic evolution of the Manitoba–Saskatchewan segment of the Paleoproterozoic Trans-Hudson Orogen, Canada. Canadian Journal of Earth Sciences, **42**: 741–759.

Aspler, B.A., and Chiarenzelli, J.R. 1998. Two Neoarchean supercontinents? Evidence from the Paleoproterozoic. Sedimentary Geology, **120**: 75–104.

Baird, D.J., Nelson, K.D., Knapp, J.H., Walters, J.J., and Brown, L.D. 1996. Crustal structure and evolution of the Trans-Hudson orogen: results from seismic reflection profiling. Tectonics, **15**: 416–426.

Barley, M.E., Bekker, A., and Krapez, B. 2005. Late Archean to Early Paleoproterozoic global tectonics, environmental change and the rise of atmospheric oxygen. Earth and Planetary Science Letters, **238**: 156–171.

Bekker, A., and Eriksson, K.A. 2003. A Paleoproterozoic drowned carbonate platform on the southeastern margin of the Wyoming craton: a record of the Kenorland breakup. Precambrian Research, **120**: 327–364.

Bekker, A., Karhu, J.A., Eriksson, K.A., and Kaufman, A.J. 2003. Chemostratigraphy of Paleoproterozoic carbonate successions of the Wyoming craton: tectonic forcing of biogeochemical change? Precambrian Research, **120**: 279–325.

Bickford, M.E., Mock, T.E., Steinhart, W.E. III, Collerson, K.D., and Lewry, J.F. 2005. Origin of the Archean Sask craton and its extent within the Trans-Hudson orogen: evidence from Pb and Nd isotopic compositions of basement rocks and post-orogenic intrusions. Canadian Journal of Earth Sciences, **42**: 659–684.

Bickford, M.E., Wooden, J.L., and Bauer, R.L. 2006. SHRIMP study of zircons from Early Archean rocks in the Minnesota River Valley: implications for the tectonic history of the Superior Province. Geological Society of America Bulletin, **118**: 94–108.

Bleeker, W. 2003. The late Archean record: a puzzle in ca. 35 pieces. Lithos, **71**: 99–134.

Bleeker, W. 2004. Taking the pulse of planet Earth; a proposal for a new multi-disciplinary flagship project in Canadian solid earth sciences. Geoscience Canada, **31**: 179–190.

Bleeker, W., and Ernst, R. 2006. Short-lived mantle generated magmatic events and their dyke swarms: the key unlocking Earth's paleogeographic record back to 2.6 Ga. *In* Dyke swarms—time markers of crustal evolution. *Edited by* E. Hanski, S. Mertanen, T. Rämö, and J. Vuollo. A.A. Balkema, Rotterdam, The Netherlands. pp. 3–26.

Brady, J.B., Kovaric, D.N., Cheney, J.T., Jacob, L.J., and King, J.T. 2004. $^{40}Ar/^{39}Ar$ ages of metamorphic rocks from the Tobacco Root Mountains region, Montana. *In* Precambrian geology of the Tobacco Root Mountains, Montana. *Edited by* J.B. Brady, H.R. Burger, J.T. Cheney, and T.A. Harms. Geological Society of America, Special Paper 377, pp. 131–149.

Buchan, K.L., Mortensen, J.K., and Card, K.D. 1993. Northeast-trending Early Proterozoic dykes of southern Superior Province: multiple episodes of emplacement recognized from integrated paleomagnetism and U–Pb geochronology. Canadian Journal of Earth Sciences, **30**: 1286–1296.

Buchan, K.L., Halls, H.C., and Mortensen, J.K. 1996. Paleomagnetism, U–Pb geochronology, and geochemistry of Marathon dykes, Superior Province, and comparison with the Fort Frances swarm. Canadian Journal of Earth Sciences, **33**: 1583–1595.

Buchan, K.L., Mertanen, S., Park, R.G., Pesonen, L.J., Elming, S.-Å., Abrahamsen, N. et al. 2000. Comparing the drift of Laurentia and Baltica in the Proterozoic: the importance of key paleomagnetic poles. Tectonophysics, **319**: 167–198.

Chamberlain, K.R. 1998. Medicine Bow orogeny: timing of deformation and model of crustal structure produced during continent-arc collision, ca. 1.78 Ga, southeastern Wyoming. Rocky Mountain Geology, **33**: 259–277.

Cheney, J.T., Webb, A.A.G., Coath, C.D., and McKeegan, K.D. 2004. In situ ion microprobe $^{207}Pb/^{206}Pb$ dating of monazite from Precambrian metamorphic suites, Tobacco Root Mountains, Montana. *In* Precambrian geology of the Tobacco Root Mountains, Montana. *Edited by* J.B. Brady, H.R. Burger, J.T. Cheney, and T.A. Harms. Geological Society of America, Special Paper 377, pp. 151–180.

Cherniak, D.J. 1993. Lead diffusion in titanite and preliminary results on the effects of radiation damage on Pb transport. Chemical Geology, **110**: 177–194.

Cox, D.M., Frost, C.D., and Chamberlain, K.R. 2000. 2.01-Ga Kennedy dike swarm, southeastern Wyoming: record of a rifted margin along the southern Wyoming Province. Rocky Mountain Geology, **35**: 7–30.

Dahl, P.S. 1997. A crystal-chemical basis for Pb retention and fission-track annealing systematics in U-bearing minerals, with implications for geochronology. Earth and Planetary Science Letters, **150**: 277–290.

Dahl, P.S., and Frei, R. 1998. Single-phase dating of coexisting garnet and staurolite in the Black Hills collisional orogen (South Dakota), with implications for Early Proterozoic tectonism. Geology, **26**: 111–114.

Dahl, P.S., and Hamilton, M.A. 2002. Ion microprobe evidence for thermotectonic reworking of the NW Archean Wyoming Province along the Great Falls tectonic zone, SW Montana, USA. Geological Association of Canada and Mineralogical Association of Canada Abstracts with Programs, **27**: 25.

Dahl, P.S., and McCombs, J.A. 2005. "Rosetta grains" of Precambrian accessory minerals, Black Hills, South Dakota: 2900–1700 Ma microprobe ages and implications for regional tectonic history. The Compass, **78**: 59–75.

Dahl, P.S., Holm, D.K., Gardner, E.T., Hubacher, F.A., and Foland, K.A. 1999. New constraints on the timing of Early Proterozoic tectonism in the Black Hills (South Dakota), with implications for the docking of the Wyoming Province with Laurentia. Geological Society of America Bulletin, **111**: 1335–1349.

Dahl, P.S., Hamilton, M.A., Stern, R.A., Frei, R., and Berg, R.B. 2000. In situ SHRIMP investigation of an Early Proterozoic metapelite: implications for Pb–Pb dating of garnet and staurolite. Geological Society of America Abstracts with Programs, **32**: 297.

Dahl, P.S., Hamilton, M.A., Jercinovic, M.J., Terry, M.P., Williams, M.L., and Frei, R. 2005*a*. Comparative isotopic and chemical geochronometry of monazite, with implications for U–Th–Pb dating by electron microprobe: an example from metamorphic rocks of the eastern Wyoming Craton. American Mineralogist, **90**: 619–638.

Dahl, P.S., Terry, M.P., Jercinovic, M.J., Williams, M.L., Hamilton, M.A., Foland, K.A., et al. 2005*b*. In situ microchronometry of metamorphic monazite (Black Hills, SD) and the timing of Paleo-

proterozoic thermotectonism in the eastern Wyoming craton. American Mineralogist, **90**: 1712–1728.

Davis, D.W., and Stott, G.M. 2003. Geochronology of two Proterozoic mafic dike swarms in northwestern Ontario. *In* Summary of fieldwork and other activities 2003. Ontario Geological Survey, Open File Report 6120, pp. 12-1–12-7.

DeWitt, E., Redden, J.A. Wilson, A.B., and Buscher, D. 1986. Mineral resource potential of the Black Hills National Forest, South Dakota and Wyoming. United States Geological Survey Bulletin 1580, 135 pp.

DeWitt, E., Redden, J.A. Wilson, A.B., and Buscher, D. 1989. Geologic map of the Black Hills area, South Dakota and Wyoming. United States Geological Survey Miscellaneous Investigation Series Map I-1910, scale 1 : 250 000.

Ernst, R.E., and Buchan, K.L. 1993. Paleomagnetism of the Abitibi dyke swarm, southern Superior Province, and implications for the Logan Loop. Canadian Journal of Earth Sciences, **30**: 1886–1897.

Ernst, R.E., and Buchan, K.L. 2001. Large mafic magmatic events through time and links to mantle-plume heads. *In* Mantle plumes: Their identification through time. *Edited by* R.E. Ernst and K.L. Buchan. Geological Society of America, Special Paper 352, pp. 483–566.

Erslev, E.A., and Sutter, J.F. 1990. Evidence for Proterozoic mylonitization in the northwestern Wyoming Province. Geological Society of America Bulletin, **102**: 1681–1694.

Foland, K.A. 1983. $^{40}Ar/^{39}Ar$ incremental heating plateaus for biotites with excessive argon. Isotope Geoscience, **1**: 1681–1694.

Foland, K.A., Linder, J.S., Laskowski, T.E., and Grant, N.K. 1984. $^{40}Ar/^{39}Ar$ dating of glauconites: measured ^{39}Ar recoil loss from well-crystallized specimens. Isotope Geoscience, **1**: 241–264.

Foland, K.A., Fleming, T.H., Heimann, A., and Elliot, D.H. 1993. Potassium-argon dating of fine-grained basalts with massive Ar loss: application of the $^{40}Ar/^{39}Ar$ technique to plagioclase and glass from the Kirkpatrick Basalt, Antarctica. Chemical Geology (Isotope Geoscience Section), **107**: 173–190.

Foster, D.A., Mueller, P.A., Mogk, D.W., Wooden, J.L., and Vogl, J. 2006. Proterozoic evolution of the western margin of the Wyoming craton: implications for the tectonic and magmatic evolution of the northern Rocky Mountains. Canadian Journal of Earth Sciences, **43**: this issue.

Frei, R., and Kamber, B.S. 1995. Single mineral Pb–Pb dating. Earth and Planetary Science Letters, **129**: 261–268.

Frei, R., Villa, I.M., Nägler, T.F., Kramers, J.D., Przybylowicz, W.J., Prozesky et al. 1997. Single mineral dating by the Pb–Pb step-leaching method; assessing the mechanisms. Geochimica et Cosmochimica Acta, **61**: 393–414.

Frost, B.R., Chamberlain, K.R., and Schumacher, J.C. 2000. Sphene (titanite): phase relations and role as a geochronometer. Chemical Geology, **172**: 131–148.

Frost, C.D. 1993. Nd isotopic evidence for the antiquity of the Wyoming Province. Geology, **21**: 351–354.

Frost, C.D., Frost, B.R., Chamberlain, K.R., and Hulsebosch, T.P. 1998. The Later Archean history of the Wyoming Province as recorded by granitic magmatism in the Wind River Range, Wyoming. Precambrian Research, **89**: 145–173.

Gosselin, D.C., Papike, J.J., Zartman, R.E., Peterman, Z.E., and Laul, J.C. 1988. Archean rocks of the Black Hills, South Dakota: reworked basement from the southern extension of the Trans-Hudson Orogen. Geological Society of America Bulletin, **100**: 1244–1249.

Halls, H.C., and Davis, D.W. 2004. Paleomagnetism and U–Pb geochronology of the 2.17 Ga Biscotasing dyke swarm, Ontario, Canada: evidence for vertical-axis crustal rotation across the Kapuskasing Zone. Canadian Journal of Earth Sciences, **41**: 255–269.

Hamilton, M.A., Davis, D.W., Buchan, K.L., and Halls, H.C. 2002. Precise U–Pb dating of reversely magnetized Marathon diabase dykes and implications for emplacement of giant dyke swarms along the southern margin of the Superior Province, Ontario. *In* Radiogenic age and isotopic studies. Geological Survey of Canada, Report 15, Current Research 2002-F6, pp. 1–8.

Hamilton, M.A., McLelland, J., and Selleck, B. 2004. SHRIMP U–Pb zircon geochronology of the anorthosite–mangerite–charnockite–granite (AMCG) suite, Adirondack mountains, New York: ages of emplacement and metamorphism. *In* Proterozoic tectonic evolution of the Grenville orogen in North America. *Edited by* R.P. Tollo, L. Corriveau, J. McLelland, and M.J. Bartholomew. Geological Society of America, Memoir 197, pp. 337–355.

Harlan, S.S. 2005. The Paleoproterozoic leopard dikes of Montana and Wyoming: a dismembered fragment of the 2.45 Ga Hearst-Matachewan giant radiating dike swarm of the Superior craton? Geological Society of America Abstracts with Programs, **37**: 505.

Harlan, S.S., Geissman, J.W., and Premo, W.R. 2003*a*. Paleomagnetism and geochronology of an Early Proterozoic quartz diorite in the southern Wind River Range, Wyoming, USA Tectonophysics, **362**: 105–122.

Harlan, S.S., Heaman, L., LeCheminant, A.N., and Premo, W.R. 2003*b*. Gunbarrel mafic magmatic event: a key 780 Ma time marker for Rodinia plate reconstructions. Geology, **31**: 1053–1056.

Heaman, L.M. 1997. Global mafic magmatism at 2.45 Ga: remnants of an ancient large igneous province. Geology, **25**: 299–302.

Hilburn, I.A., Kirschvink, J.L., Tajika, E., Tada, R., Hamano, Y., and Yamamoto, S. 2005. A negative fold test on the Lorrain Formation of the Huronian Supergroup: uncertainty on the paleolatitude of the Paleoproterozoic Gowganda glaciation and implications for the great oxygenation event. Earth and Planetary Science Letters, **232**: 315–332.

Holm, D.K., Dahl, P.S., and Lux, D.R. 1997. $^{40}Ar/^{39}Ar$ evidence for Middle Proterozoic (1300–1500) slow cooling of the southern Black Hills, South Dakota: implications for Proterozoic P–T evolution and post-tectonic magmatism. Tectonics, **16**: 609–622.

Holm, D.K., Van Schmus, W.R., MacNeill, L.C., Boerboom, T.J., Schweitzer, D., and Schneider, D. 2005. U–Pb zircon geochronology of Paleoproterozoic plutons from the northern mid-continent, USA: evidence for subduction flip and continued convergence after geon 18 Penokean orogenesis. Geological Society of America Bulletin, **117**: 259–275.

Ireland, T.R., and Williams, I.S. 2003. Considerations in zircon geochronology by SIMS. *In* Zircon. *Edited by* J.M. Hanchar and P.W.O. Hoskins. Reviews in Mineralogy and Geochemistry, **53**: 215–241.

James, R.S., Easton, R.M., Peck, D.C., and Hrominchuk, J.L. 2002. The East Bull Lake Intrusive Suite: remnants of a ~2.48 Ga large igneous and metallogenic province in the Sudbury area of the Canadian Shield. Economic Geology, **97**: 1577–1606.

Jones, C.L., Dahl, P.S., Wooden, J.L., Mazdab, F.K., and Tracy, R.J. 2004. Geochronology of U-bearing accessories from Precambrian metamorphic rocks, Ruby Range, SW Montana: deciphering geological events that shaped the NW Wyoming Province. Geological Society of America Abstracts with Programs, **36**: 568.

Kellogg, K.S., Snee, L.W., and Unruh, D.M. 2003. The Mesoproterozoic Beaverhead impact structure and its tectonic setting, Montana–Idaho: $^{40}Ar/^{39}Ar$ and U–Pb isotopic constraints. Journal of Geology, **111**: 639–652.

Lisenbee, A.L. 1978. Laramide structure in the Black Hills Uplift,

South Dakota – Wyoming – Montana. *In* Laramide folding associated with basement block faulting in the western United States. *Edited by* V. Matthews. Geological Society of America Memoir 151, pp. 165–169.

Loehn, C.W. III, Dahl, P.S., Tracy, R.J., Wooden, J.L., and Mazdab, F.K. 2004. U–Pb geochronology of monazite and zircon in Archean metamorphic rocks from the South Madison and Beartooth Ranges, SW Montana, with implications for thermotectonic evolution of the Wyoming Province. Geological Society of America Abstracts with Programs, **36**: 568–569.

Ludwig, K.R. 2001. SQUID 1.00, a user's manual. Berkeley Geochronology Center Special Publication No. 2.

Ludwig, K.R. 2003. Isoplot 3.00, a geochronological toolkit for Excel. Berkeley Geochronology Center Special Publication No. 4.

McCombs, J.A. 2002. Geochronology of Precambrian basement and adjacent rocks, Black Hills, South Dakota. Unpublished Masters thesis, Kent State University, Kent, Ohio.

McCombs, J.A., Dahl, P.S., and Hamilton, M.A. 2004. U–Pb ages of Neoarchean granitoids from the Black Hills, South Dakota, USA: implications for evolution of the Archean Wyoming Province. Precambrian Research, **130**: 161–184.

Mertanen, S., Halls, H.C., Vuollo, J.I., Pesonen, L.J., and Stepanov, V.S. 1999. Paleomagnetism of 2.44 Ga mafic dykes in Russian Karelia, eastern Fennoscandian Shield—implications for continental reconstructions. Precambrian Research, **98**: 197–221.

Mogk, D.W., Mueller, P.A., and Wooden, J.L. 1992. The nature of Archaean terrane boundaries: an example from the northern Wyoming Province. Precambrian Research, **55**: 155–168.

Mueller, P.A., and Wooden, J.L. 1988. Evidence for Archean subduction and crustal recycling, Wyoming Province. Geology, **16**: 871–874.

Mueller, P., Heatherington, A., D'Arcy, K., Wooden, J., and Nutman, A. 1996. Constrasts between Sm–Nd and U–Pb zircon systematics in the Tobacco Root batholith, Montana: implications for determination of crustal age provinces. Tectonophysics, **265**: 169–179.

Mueller, P.A., Heatherington, A.L., Kelly, D.M., Mogk, D.W., and Wooden, J.L. 2002. Paleoproterozoic crust within the Great Falls tectonic zone: implications for the assembly of southern Laurentia. Geology, **30**: 127–130.

Mueller, P.A., Burger, H.R., Wooden, J.L., Heatherington, A.L., Mogk, D.W., and D'Arcy, K. 2004. Age and evolution of Precambrian fabrics and structures in the Tobacco Root Mountains, Montana. *In* Precambrian geology of the Tobacco Root Mountains, Montana. *Edited by* J.B. Brady, H.R. Burger, J.T. Cheney, and T.A. Harms. Geological Society of America, Special Paper 377, pp. 181–202.

Nabelek, P.I., Liu, M., and Sirbescu, M. 2001. Thermo-rheological, shear heating model for leucogranite generation, metamorphism, and deformation during the Proterozoic Trans-Hudson orogeny, Black Hills, South Dakota. Tectonophysics, **342**: 371–388.

Pesonen, L.J., Elming, S.-Å., Mertanen, S., Pisarevsky, S., D'Agrella-Filho, M.S., Meert, J.G. et al. 2003. Palaeomagnetic configuration of continents during the Proterozoic. Tectonophysics, **375**: 289–324.

Premo, W.R., and Van Schmus, W.R. 1989. Zircon geochronology of Precambrian rocks in southeastern Wyoming and northern Colorado. *In* Proterozoic geology of the Southern Rocky Mountains. *Edited by* J.A. Grambling and B.J. Tewksbury. Geological Society of America, Special Paper 335, pp. 13–32.

Rayner, N.M., Stern, R.A., and Bickford, M.E. 2005. Tectonic implications of new SHRIMP and TIMS U–Pb geochronology of rocks from the Sask Craton, Peter Lake Domain, and Hearne margin, Trans-Hudson Orogen, Saskatchewan. Canadian Journal of Earth Sciences, **42**: 635–657.

Redden, J.A. 1981. Summary of the geology of the Nemo area. *In* Geology of the Black Hills, South Dakota and Wyoming. *Edited by* F.J. Rich. Geological Society of America Guidebook, American Geological Institute, Falls Church, Va., pp. 193–210.

Redden, J.A. 1987. Early Proterozoic and Precambrian-Cambrian unconformities of the Nemo area, Black Hills, South Dakota. *In* Centennial field guide. Vol. 2. *Edited by* S.S. Beus. Geological Society of America, Rocky Mountain Section, Denver, Colo. pp. 219–225.

Redden, J.A., Peterman, Z.E., Zartman, R.E., and DeWitt, E.R. 1990. U–Th–Pb geochronology and preliminary interpretation of Precambrian events in the Black Hills, South Dakota. *In* The Trans-Hudson orogen. *Edited by* J.F. Lewry and M.R. Stauffer. Geological Association of Canada, Special Paper 37, pp. 229–251.

Roberts, H., Dahl, P., Kelley, S., and Frei, R. 2002. New ^{207}Pb–^{206}Pb and ^{40}Ar–^{39}Ar ages from SW Montana, USA: constraints on the Proterozoic and Archaean tectonic and depositional history of the Wyoming Province. Precambrian Research, **117**: 119–143.

Roscoe, S.M., and Card, K.D. 1993. The reappearance of the Huronian in Wyoming: rifting and drifting of ancient continents. Canadian Journal of Earth Sciences, **30**: 2475–2480.

Schaller, M., Steiner, O., Studer, I., Frei, R., and Kramers, J.D. 1997. Pb stepwise leaching (PbSL) dating of garnet—addressing the inclusion problem. Schweizerische Mineralogische Petrographische Mitteilungen, **77**: 113–121.

Schmitz, M.D., Bowring, S.A., Southwick, D.L., Boerboom, T.J., and Wirth, K.R. 2006. High-precision U–Pb geochronology in the Minnesota River Valley subprovince and its bearing on the Neoarchean to Paleoproterozoic evolution of the southern Superior Province. Geological Society of America Bulletin, **118**: 82–93.

Sears, J.W., and Price, R.A. 2003. Tightening the Siberia connection to western Laurentia. Geological Society of America Bulletin, **115**: 943–953.

Shaw, C.S.J., Young, G.M., and Fedo, C.M. 1999. Sudbury-type breccias in the Huronian Gowganda Formation near Whitefish Falls, Ontario: products of diabase intrusion into incompletely consolidated sediments? Canadian Journal of Earth Sciences, **36**: 1435–1448.

Sims, P.K., Card, K.D., Morey, G.B., and Peterman, Z.E. 1980. The Great Lakes tectonic zone—a major crustal structure in central North America. Geological Society of America Bulletin, **91**: 690–698.

Southwick, D.L., and Chandler, V.W. 1996. Block and shear-zone architecture of the Minnesota River Valley subprovince: implications for late Archean accretionary tectonics. Canadian Journal of Earth Sciences, **33**: 831–847.

Southwick, D.L., and Day, W.C. 1983. Geology and petrology of Proterozoic mafic dikes, north-central Minnesota and western Ontario. Canadian Journal of Earth Sciences, **20**: 622–638.

Stern, R.A. 1997. The GSC sensitive high resolution ion microprobe (SHRIMP): analytical techniques of zircon U–Th–Pb age determinations and performance evaluation. *In* Radiogenic age and isotopic studies. Geological Survey of Canada, Current Research 1997-F, Report 10, pp. 1–31.

Stern, R.A., and Amelin, Y. 2003. Assessment of errors in SIMS zircon U-Pb geochronology using a natural zircon standard and NIST SRM 610 glass. Chemical Geology, **197**: 111–146.

Tinkham, D.K., and Marshak, S. 2004. Precambrian dome-and-keel structure in the Penokean orogenic belt of northern Michigan, USA. *In* Gneiss domes in orogeny. *Edited by* D.L. Whitney, C.

Teyssier, and C.S. Siddoway. Geological Society of America, Special Paper 380, pp. 321–338.

Walker, R.J., Hanson, G.N., Papike, J.J., and O'Neil, J.R. 1986. Nd, O and Sr isotopic constraints on the origin of Precambrian rocks, Southern Black Hills, South Dakota. Geochimica et Cosmochimica Acta, **50**: 2833–2846.

Weil, A.B., Van der Voo, R., MacNiocaill, C., and Meert, J.G. 1998. The Proterozoic supercontinent Rodinia: paleomagnetically derived reconstructions for 1100–800 Ma. Earth and Planetary Science Letters, **154**: 13–24.

Williams, H., Hoffman, P.F., Lewry, J.F., Monger, J.W.F., and Rivers, T. 1991. Anatomy of North America: thematic portrayals of the continent. Tectonophysics, **187**: 117–134.

Williams, I.S. 1997. U–Th–Pb geochronology by ion microprobe: not just ages but histories. Society of Economic Geologists Reviews in Economic Geology, **7**: 1–35.

Wintsch, R.P., Aleinikoff, J.N., and Yi, K. 2005. Foliation development and reaction softening by dissolution and precipitation in the transformation of granodiorite to orthogneiss, Glastonbury Complex, Connecticut, USA. The Canadian Mineralogist, **43**: 327–347.

Wirth, K.R., Vervoort, J.D., and Heaman, L.M. 1995. Nd isotopic constraints on mantle and crustal contributions to 2.08 Ga diabase dykes of the southern Superior Province. *In* Proceedings of the 3rd International Dyke Conference, Jerusalem, Program and Abstracts, p. 84.

Woo, C.C. 1952. The Pre-Cambrian geology and amphibolites of the Nemo district, Black Hills, South Dakota. Unpublished Ph.D. dissertation, University of Chicago, Il. 148 pp.

Wooden, J.L., and Mueller, P.A. 1988. Pb, Sr, and Nd isotopic compositions of a suite of Late Archean, igneous rocks, eastern Beartooth Mountains: implications for crust-mantle evolution. Earth and Planetary Science Letters, **87**: 59–72.